Eur Biophys J (2006) 35: 104–124
DOI 10.1007/s00249-005-0013-y

REVIEW

Grace Brannigan · Lawrence C.-L. Lin
Frank L. H. Brown

Implicit solvent simulation models for biomembranes

Received: 20 May 2005 / Revised: 3 August 2005 / Accepted: 12 August 2005 / Published online: 27 September 2005

Abstract Fully atomic simulation strategies are infeasible for the study of many processes of interest to membrane biology, biophysics and biochemistry. We review various coarse-grained simulation methodologies with special emphasis on methods and models that do not require the explicit simulation of water. Examples from our own research demonstrate that such models have potential for simulating a variety of biologically relevant phenomena at the membrane surface.

Introduction

Biomembranes play a central role in most processes in cellular biology (Lodish et al. 1995; Gennis 1989), and lipid bilayer membranes are becoming increasingly important for technological applications and medicine (Tien and Ottova-Leitmannova 2003). From a purely physical standpoint, lipid bilayers are a fascinating system for study because of their complex properties over a range of different sizes and time regimes. The clear importance of membranes across a range of disciplines has led to extensive study of lipids and bilayers from both experimental and theoretical perspectives (Bloom et al. 1991; Evans and Skalak 1980; Lipowsky and Sackmann 1995; Nagle and Tristram-Nagle 2000).

Computationally, atomistic simulations of lipid bilayers have provided insight into the microscopic structure within the membrane sheet (of lipids, cholesterol and water) and allowed for realistic simulation of transmembrane proteins in their native environment (Chiu et al. 2002; Feller 2000; Marrink et al. 1993; Pastor 1994; Pitman et al. 2005; Smondyrev and Berkowitz 1999; Tobias et al. 1997). However, the time scale and size limitations of fully atomic molecular dynamics (MD) simulation currently preclude detailed studies involving mixing of multiple lipid species, interactions between multiple proteins in a membrane environment, verification of "macroscopic" elastic properties (without finite size artifacts) and essentially any phenomena occurring over lengths larger than tens of nanometers and/or times longer than tens of nanoseconds. Since much biological behavior relies on complex inhomogeneous membrane environments and interactions spanning a range of length and time scales, such limitations are severe.

It is worth examining just how severe these limitations really are. A recent paper by Feller and co-workers reported MD simulation of a single rhodopsin protein in a membrane environment consisting of water, two lipid species and cholesterol for a total time of 118 ns (Pitman et al. 2005). The simulation box employed had dimensions of $5.5\times7.7\times10$ nm^3 (43,222 atoms). We do not claim this to be the largest MD simulation on record, but the authors themselves note that the simulation was only possible because of "recent improvements in computer power and simulation techniques." We take this study as a benchmark for what is feasible with current MD and computer technologies. Let us imagine that MD computation scales linearly with system size regardless of how massive the simulation. Then, a reasonable estimate of "computing power" necessary to run a given simulation is given by the size of the simulation volume (i.e., number of atoms) times the duration of the simulation. By this definition, the benchmark simulation above required about 50,000 ns nm^3 of MD computing power.

Suppose we were interested in simulating a small fraction of the surface of a cell, a 1 μm×1 μm patch (for reference, a red blood cell is approximately 7 μm in diameter) for a time of 1 ms. To allow for out-of-plane

G. Brannigan · L. C.-L. Lin
Department of Physics and Astronomy, University of California, Santa Barbara, CA 93106-9530, USA

F. L. H. Brown (✉)
Department of Chemistry and Biochemistry, University of California, Santa Barbara, CA 93106-9510, USA
E-mail: flbrown@chem.ucsb.edu

membrane undulations (see below), we set the dimension of the box normal to the membrane surface at 100 nm. The computing power required for this simulation would be 10^{14}ns nm^3, two billion times that required for the "state-of-the-art" calculation mentioned above! Although improvement of MD simulation capability over time is impossible to predict, it seems highly unlikely that improvement will surpass Moore's (1985) law for the predicted exponential growth rate of CPU speed. Assuming (a la Moore) that MD capabilities will double every 1.5 years, our hypothetical simulation would only become feasible 46 years from now.

The above estimate is not expected to be quantitatively accurate. However, we emphasize that the simplifications introduced (linear scaling, Moore's law) are likely to fail in the direction of predicting a future that is overly optimistic. A more refined treatment would almost certainly predict that it will be much more than 46 years in the future when it becomes possible to run MD on micrometer scales for millisecond durations. From a biological point of view, these scales are actually quite conservative (see Protein mobility on the red blood cell) although it is clear that simulation of such processes with atomic scale resolution will continue to be computationally prohibitive for many years to come.

The practical limitations of fully atomic simulations have led to interest in developing model systems that preserve the physical properties of biomembranes, but with reduced computational cost. Various levels of coarse-graining have been introduced (Shelley and Shelley 2000) as will be summarized below. Explicit simulation of water in biomolecular simulations typically increases the simulation size by an order of magnitude or more relative to the size of the solute(s) (Feig and Brooks 2004). Clearly, eliminating the direct simulation of solvent is a huge computational advantage if it is possible to do so while preserving physical reality.

The evolution of membrane simulation methodologies that do not require explicit simulation of water is the primary focus of this review. We realize that the adjective "implicit" has come to mean a variety of different things to various researchers. Our own definition is borrowed straight from the dictionary, which defines implicit to mean "involved in the nature or essence of something though not revealed, expressed or developed" (Gove 1970). Any form of solvent, no matter how coarse grained, removes a model from consideration as an "implicit solvent model" in our opinion. We further narrow the focus of this review to cover two specific flavors of the model, each appropriate to a different size regime. First, we consider dynamic elastic models where the influence of water is incorporated through implicit treatment of the hydrodynamics for the solvent surrounding the bilayer. Second, we consider coarse-grained molecular level models where the stability of the bilayer (due to hydrophobic interactions in the real system) is enforced by effective lipid–lipid interactions. These interactions, though not typically derived from microscopic considerations, should be viewed as potentials of mean force, reflecting the implicit role of solvent in these simulations. Prior literature has referred to such models as "solvent-free" (Brannigan and Brown 2004) and "water-free" (Farago 2003) in addition to the moniker "implicit solvent." All such titles mean the same thing: solvent is not simulated on the computer, even though all these systems are intended to model lipid bilayers in aqueous solution. At present, these models are used primarily in Monte Carlo simulations, so the role of implicit solvent here is solely to maintain membrane integrity and reproduce thermal behavior. Hydrodynamics are not currently incorporated into this second class of models.

We note that the above definition of implicit could technically include models beyond those reviewed here. Our focus is on models that allow for general (non-planar) membrane configurations and is driven by an interest in the behavior and properties of the three-dimensional membrane itself. Another class of implicit solvent models regard the bilayer solely as a planar environment whose dielectric properties influence protein stability (Im et al. 2003). Such models are interesting in the context of protein behavior, but fall outside the scope of this review. Similarly, models that treat the membrane as a flat two-dimensional fluid (for instance, Murtola et al. 2004) hold great promise for addressing certain questions, such as domain formation in perfectly flat geometries, but also fall outside the purview of this review.

Overview of coarse-grained simulation models

Continuum models

For physical questions involving sufficiently long length and time scales, continuum models provide the only feasible simulation schemes. By coarse-graining over the lipid degrees of freedom, fluid membranes have been successfully described by infinitely thin, continuous sheets with curvature elastic energy. The solvent never appears in such a picture, although its effects are implicitly present in the elastic properties that specify the model. Canham (1970) first used such a model to show that curvature energy minimization leads to the various observed shapes of red blood cells under different conditions. Subsequently, models developed by Helfrich included spontaneous curvature of the membrane due to differences in the composition of the two leaflets (Helfrich 1973) leading to explanations of other observed shapes in vesicles (Deuling and Helfrich 1976). Further extensions have provided detailed phase diagrams for red blood cells (Lim et al. 2002; Mukhopadhyay et al. 2002), vesicles (Lipowsky 1991; Seifert et al. 1991), as well as predictions for budding and vesiculation (Miao et al. 1991, 1994).

The Helfrich model has been most widely applied to the study of bilayers with small thermal height fluctuations away from a flat reference configuration (Safran

1994). Analytically, the model contains only two experimentally measured parameters, the bending rigidity and surface tension of the sheet, and allows for exact solutions that have been verified in a variety of studies. Comparisons between theory and experiment for the mean square height fluctuations in red blood cells have been successfully made (Zilker et al. 1992). Predictions of undulation-induced, steric repulsive interactions between proximal membranes (Helfrich 1978) have been verified in stacks of lipid bilayers (Safinya et al. 1989). Helfrich models with additional harmonic interactions can also be handled analytically. Equilibrium properties can be calculated for various forms of harmonic potentials (Gov and Safran 2004; Gov et al. 2003; Lin and Brown 2004b) including localized pinning and uniform confinement.

Non-harmonic potentials within the Helfrich picture have been studied through the use of Monte Carlo. Average height fluctuations and pressures have been calculated and compared to experiment by simulating stacks of lipid bilayers interacting through van der Waals attraction and repulsive hydration potentials (Gouliaev and Nagle 1998a, b). Various other non-harmonic interactions have been studied such as unbinding transitions for membranes interacting through a finite square well potential (Lipowsky and Zielenska 1989) and membranes interacting with a surface through approximate entropic, repulsive potentials (Bar-Ziv et al. 1995; Weikl and Lipowsky 2000).

Dynamics for Helfrich membranes depend upon the viscous fluid environment surrounding the bilayer. Overdamped equations of motion for the thin sheet can be derived from the Navier–Stokes equations in the same way that one derives dynamics for a collection of interacting Brownian particles (Doi and Edwards 1986). The surrounding fluid is assumed to be incompressible and inertial effects are generally negligible, leading to low Reynolds number (Stokesian) dynamics. Small fluctuations away from a flat bilayer are also assumed. Boundary conditions dictate the form of the solutions, but the fluid is generally assumed to be infinite (Doi and Edwards 1986; Granek 1997) or bounded by a wall (Brochard and Lennon 1975; Gov et al. 2004; Seifert 1994) depending upon the physical situation. Thermal fluctuations are included by adding a Langevin-like noise term to satisfy the fluctuation–dissipation relationship (Granek 1997).

Various dynamic properties of lipid bilayer systems have been successfully studied analytically using these methods. The flicker effect of red blood cells was explained on the basis of thermal undulations of the membrane surface (Brochard and Lennon 1975). Furthermore, the structure factor of stacks of membranes as a function of wave vector and frequency has been calculated and compared favorably with experiment (Zilman and Granek 1996). Harmonic interactions can generally be handled analytically for the dynamics of Helfrich sheets. The effects of the coupling between the red blood cell bilayer and spectrin cytoskeleton have been modeled through an effective surface tension and harmonic confinement, as well as a wall boundary condition for the hydrodynamics (Gov et al. 2003). This theory has provided improved fits to experimental measurements (Zilker et al. 1987) of the frequency dependence of the mean square height amplitude. Analytical results have also been found for the time correlation functions for a membrane in a localized harmonic potential, and experiments for optical tweezers have been suggested (Granek and Klafter 2001).

Few dynamical studies on systems containing non-harmonic interactions have been performed. Studies of the formation of the immunological synapse have included Helfrich elasticity (Qi et al. 2001), but without the need for hydrodynamics or thermal fluctuations. For polymers adsorbed on surfaces, dynamics simulations (Laradji 1999), numerical solutions (Laradji 2002) and Monte Carlo simulations (Laradji 2004) have predicted the scaling of excess rigidity with the grafted polymer density. Recently, our work has focused on a simulation algorithm we have termed Fourier space Brownian dynamics (FSBD; Lin and Brown 2004a). Our method is a prescription for the time evolution of the lipid bilayer in the presence of arbitrary forces and includes hydrodynamics as well as thermal fluctuations. The FSBD algorithm is sufficiently general to find application to many biophysical processes. We discuss the algorithm and various applications in Fourier space Brownian dynamics.

Particle-based models

For many questions regarding lipid bilayers, a continuum formulation is inappropriate. The models described above are suitable for studying long-wavelength undulation behavior in specific geometries with elastic properties provided as inputs to the model. For simulations at smaller scales, in more general geometries or aimed at predicting elastic properties, particle-based methods are more versatile. In practice, simulation particles may represent single atoms, groups of atoms, single lipids or multiple lipids. Stability of the bilayer structure within such models may be accomplished by constraining such a geometry (tethered models) or as a natural consequence of interparticle interactions. Models that include solvent particles are able to enforce bilayer stability in the same general method adopted by nature (hydrophobic attractions). In the absence of explicit solvent, the hydrophobic effect must be incorporated through effective potentials between membrane particles.

Tethered models

A wide class of solvent-free particle-based models maintain membrane integrity by ‘‘tethering’’: particles are either bound to each other or to the same continuous sheet. In the former case, models resemble the elastic

picture discussed previously in the sense that Helfrich energetics are imposed with elastic properties assigned as input to the model. The advantage is that one may simulate geometries with a tethered model that might be impossible to treat analytically. For a review of earlier applications, see Gompper and Kroll (1997); recently such "tethered membranes" have been used to study vesicle budding (Kohyama et al. 2003; Kumar et al. 2001; Kumar and Rao 1998), inclusions (Holzöhner and Schoen 1999), vesicle adhesion (Gruhn and Lipowsky 2005), coupling between curvature and composition (McWhirter et al. 2004) and vesicle behavior in shear flow (Noguchi and Gompper 2004). The simulations of Ayton and Voth (2002) constitute a special case; while dissipative particle dynamics (DPD) is employed, the model "bonds [DPD] particles in a two-dimensional (2D) network." The compressibility modulus k_A for the DPD membrane particles is matched to simulations of an atomistic solvated system; however, the bending modulus k_c is not an input to the model. In other words, Helfrich elasticity is not imposed, but falls out of this particular tethered system.

Another class of tethered models constrain the heads of flexible lipids to one or two common sheets, rather than tethering point particles to each other. These systems have been primarily used to investigate chain conformations (Harries and Ben-Shaul 1997), depletion forces (Sintes and Baumgärtner 1998a, b) and related properties (Whitehead et al. 2001) within a flat bilayer geometry. Recently Laradji (2004) has allowed the sheet to fluctuate according to the Helfrich elastic model.

Non-tethered solvated models

The field of coarse-grained lipid models is large and growing. The majority of approaches adopted in the literature are not based on implicit solvent, but rather include water in various approximate, particle-based forms. A comprehensive review of all models falling into this category would merit a stand-alone review in its own right, but this subject matter is perpendicular to our focus here. We include the few brief words below only to point out that implicit solvent models are certainly not the only route to adopt in lipid simulations. Indeed, most workers would argue that explicit solvent models are the most realistic and general coarse-grained models developed to date.

Solvated coarse-grained models for lipids can be divided into two general categories. Some models are developed from bottom-up, starting with atomic resolution and simplifying the description while attempting to maintain certain microscopic/mesoscopic properties of the lipids, water and other molecules. Other models have been developed from top-down in order to reproduce continuum and mesoscopic properties of the membrane without microscopic details ever being explicitly considered. Models in the former category (Izvekov and Voth 2005; Marrink et al. 2004; Shelley et al. 2001) typically use a hierarchical algorithm for integrating atomic degrees of freedom. (To our knowledge, this top-down approach has never been applied to implicit solvent models.) Models in the latter category (Ayton et al. 2001; Goetz and Lipowsky 1998; Groot and Rabone 2001; Laradji and Kumar 2004; Rekvig et al. 2003; Shillcock and Lipowsky 2002; Smit et al. 1991; Soddemann et al. 2001; Stevens 2004; Yamamoto et al. 2002;) tend to rely on ad hoc potentials, sacrificing microscopic detail for the sake of simplicity and speed. Both schemes have their own advantages, and application of one model over another is mostly dependent upon the particular applications one is interested in. From the standpoint of biology and biochemistry, the bottom-up approach has a lot of potential. It may eventually become possible to run realistic simulations of bilayers incorporating multiple lipid species, cholesterol, proteins, etc., without the computational cost inherent to fully atomic molecular dynamics. From the standpoint of physics and biophysics, the top-down approaches are appealing in their ability to study long-wavelength behavior and fundamental questions about membrane biophysics. It is these top-down models that implicit solvent models have the most in common with at present. Argument can be made that if ad hoc potentials are already present in a solvated model, then it makes sense to try to incorporate all solvent effects within effective interactions between lipids. This is the primary motivation behind the implicit solvent models discussed in Applications of molecular models.

Detailing the numerous approaches to coarse-graining is outside the scope of this review, and here we simply outline the premise behind the solvated top-down models. Most have extended the hydrophobic/polar (HP) scheme used in polymer simulations (Dill et al. 1995; Kolinski and Skolnick 2004 and references therein). "Polar" beads make up the solvent, while one or two short "hydrophobic" chains attached to a polar head bead represents a lipid. Polar beads prefer other polar beads over hydrophobic beads, inducing membrane formation. The form of the potentials vary from model to model, as do the molecular complexity and the intramolecular constraints. In these coarse-grained models, explicit solvent provides a straightforward and physically motivated, but computationally expensive, mechanism for inducing membrane aggregation.

Non-tethered implicit solvent models

Effective attractions between lipids are necessary to induce membrane aggregation in implicit solvent models. A common obstacle (Drouffe et al. 1991; Noguchi and Takasu 2001b) encountered by developers has been the tendency (Cooke et al. 2005) of standard attractive forms (i.e., van der Waals) to crystallize the membrane, i.e., the phase diagram for an assembly of such lipids does include a bilayer structure, but these structures are not fluid at any temperature. At sufficiently high tem-

peratures the bilayer sublimes without ever passing through a fluid phase. Consequently, successful interactions have leaned towards the exotic, and early efforts (Drouffe et al. 1991; Noguchi and Takasu 2001b) implied that many-body potentials were necessary to access a fluid regime.

The pioneering model of Drouffe, Maggs and Leibler (Drouffe et al. 1991) was used in an early simulation study of membrane undulations. In this model, anisotropic spheres (Fig. 1a) interact through both orientation-dependent pair potentials and an isotropic many-body potential. The many-body potential is minimized when a molecule has six nearest neighbors, and the orientation-dependent potential encourages these six nearest neighbors to lie in the same plane. Extremely efficient, the model was used to self-assemble a vesicle 10 years before a (much smaller) atomistic bilayer (Marrink et al. 2001) was assembled. Furthermore, the membrane undulations were used to extract the bending rigidity k_c; it took 8 years before a similar measurement (Goetz et al. 1999) of k_c from a simulated solvated membrane was published.

A successor to the Drouffe, Maggs and Leibler model, the Noguchi and Takasu model (Noguchi and Takasu 2001b) uses many-body potentials among molecules with a slightly more complex (and conventional) architecture. Each lipid is represented by a rigid chain of three beads (Fig. 1b); the many-body potential is applied to the two hydrophobic beads. This model has been used to study self-assembly of vesicles (Noguchi and Takasu 2001b), vesicle fusion (Noguchi 2002; Noguchi and Takasu 2001a), adhesion of nanoparticles to vesicles (Noguchi and Takasu 2002a), pulled vesicles (Noguchi and Takasu 2002b) and crystalline vesicles (Noguchi 2003). Very recently, Wang and Frenkel (2005) have extended this model to flexible molecules.

Later successes (Brannigan and Brown 2004; Brannigan et al. 2005; Cooke et al. 2005; Farago 2003) with pair potentials demonstrated that a many-body potential was not essential for stable fluid behavior. From a practical standpoint, a strong argument can be made for the development of pair-potential models. With pair potentials, Monte Carlo algorithms are more efficient and standard packages (such as GROMACS) can be used for dynamics. Still, difficulties in accessing a fluid phase impeded development of simple implicit solvent models. While some early implicit solvent models (Edwards et al. 1998; Morikawa and Saito 1994) for surfactants used only pair potentials, these models did not demonstrate fluid behavior.

Like the Noguchi and Takasu model (Noguchi and Takasu 2001b) [and the Soddemann, Dunweg and Kremer solvated model (Soddemann et al. 2001)] the Farago model (Farago 2003) treats each lipid as a rigid chain of three beads, one polar and two hydrophobic (Fig. 1b). Unlike earlier models, the Farago model relies only upon pair interactions between lipids. This model has been used to investigate pores (Farago 2003) and a microscopic method for calculating the bending rigidity

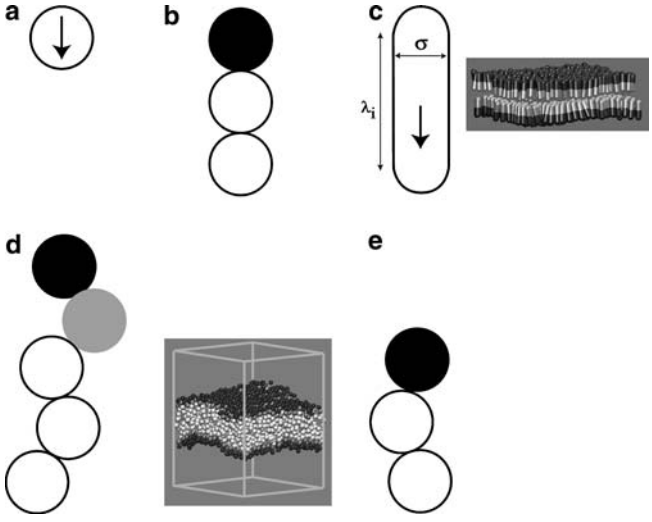

Fig. 1 Molecular architecture in various solvent-free non-tethered models. In chain molecules, hydrophobic beads are *white*, interface beads *gray* and polar beads *black*. **a** Drouffe, Maggs and Leibler model (Drouffe et al. 1991): lipids are represented by oriented spheres that interact through both pairwise and many-body potentials. **b** Rigid chains of three beads are used in both the Noguchi and Takasu many-body model (Noguchi and Takasu 2001b) and the Farago pairwise model (Farago 2003). **c** Brannigan and Brown rigid model (Brannigan and Brown 2004): one spherocylinder represents one lipid, with the normal pointing toward the "hydrophobic" end. All interactions are pairwise. Each molecule i has total tip-to-tip length $\lambda_i + \sigma$. A bilayer composed of 1,436 lipids is also shown. **d** Brannigan and Brown flexible model (Brannigan et al. 2005). This pairwise model concentrates the "hydrophobic" effect in the *gray* interface beads. Simulations discussed in this review use five bead lipids, but modification to longer lipids with more hydrophobic beads is straightforward. A bilayer composed of 800 lipids is also shown; it is considerably more flexible than the bilayer composed of rigid molecules. **e** Cooke, Kremer and Deserno model (Cooke et al. 2005). Tail beads attract each other through a soft interaction with adjustable range. Similar architecture is used in the Wang and Frenkel model (Wang and Frenkel 2005), in which the hydrophobic beads interact via a many-body potential

(Farago 2004). With some similarity to the Drouffe, Maggs and Leibler model (Drouffe et al. 1991), a rigid model developed by two of us (Brannigan and Brown 2004) treats each lipid as a soft amphiphilic rod (Fig. 1c) and will be detailed in Applications of molecular models.

This first generation of solvent-free pair interaction models did not reproduce quantitative elastic behavior. Both Farago's (Farago 2003) model and our rigid (Brannigan and Brown 2004) model produce membranes with bending rigidities k_c more similar to bilayers containing cholesterol [$k_c \sim$ 30–100k_BT (Seifert and Lipowsky 1995)] than single component model membranes [$k_c \sim$ 5–25k_BT (Seifert and Lipowsky 1995)]. As shown in Fig. 10a, the bending rigidity of our rigid model can be tuned via the rod aspect ratio, but interpolation places the region of biological relevance at thicknesses for which no stable fluid regime was observed. Furthermore, while the bending rigidity was found to decrease with the addition of a second species (Fig. 10b), we found it impossible to generate a membrane that is thermody-

namically stable in the fluid phase with elastic constants as low as those mentioned above ($k_c \sim$ 5–25k_BT).

The flexible model developed by two of us (Brannigan et al. 2005) and the Cooke, Kremer and Deserno model (Cooke et al. 2005) comprise a very recent second generation of pair-additive implicit solvent models. These models allow for molecular flexibility and have demonstrated bending elasticity in the range of biological relevance. Both are made up of flexible chains of spheres. Like the Wang and Frenkel model, the Cooke, Kremer and Deserno model uses one polar and two hydrophobic beads (Fig. 1e). Our model includes a third species: the interface bead (Fig. 1d) with a total of five beads (one polar, one interface, three hydrophobic).

A unique property of our flexible model is that it treats hydrocarbon groups at the "water"–hydrophobic interface distinctly from hydrocarbon groups in the bilayer core. In contrast, other models employ identical hydrophobic attraction among all hydrophobic beads. Although empirical in form, our interfacial attraction effectively mimics the essence of the hydrophobic effect within a bilayer geometry. This claim is supported by the range of physical behaviors effectively reproduced with this model as detailed in Thickness and heterogeneity.

Fourier space Brownian dynamics

Model and simulation algorithm

The application of continuum models to membrane-related processes is necessary when length and time scales of interest are beyond those achievable by atomistic or particle-based simulations. In these continuum models, the lipid bilayer is treated as an infinitely thin sheet where the interactions between lipids are smoothed out in favor of a bending elastic energy at each point on the membrane. The fluidity of the bilayer implies rotational symmetry and enforces certain conditions on the form of the curvature elastic energy density. The resulting formula is the Helfrich elastic energy that contains terms expanded to second order in the curvature (Helfrich 1973; Safran 1994)

$$H_{\text{bend}} = 2k_c \int \mathrm{d}\mathbf{S}[\bar{H}(\mathbf{S}) - c_0(\mathbf{S})]^2, \tag{1}$$

where $\mathbf{S}$ is a point on the surface of the membrane, c_0 a spontaneous curvature, $\bar{H}$ the mean curvature and k_c the bending modulus. (Experts will note that we have neglected the saddle-splay term since we only intend to study permanently closed or infinitely periodic surfaces.) The form above is useful for predicting the shapes of various types of closed bilayer systems (Canham 1970; Deuling and Helfrich 1976; Lim et al. 2002; Lipowsky 1991; Miao et al. 1991, 1994; Mukhopadhyay et al. 2002; Seifert et al. 1991) and studying fluctuations about spherical shapes through decomposition in spherical harmonics (Milner and Safran 1987; Safran 1983; Schneider et al. 1984; Zeman et al. 1990). In general, the membrane can also have a surface tension γ with energy

$$H_{\text{surf}} = \gamma \int \mathrm{d}\mathbf{S}. \tag{2}$$

We focus on quasiflat membranes since they encompass the majority of theoretical studies to date. In this case, the most useful parameterization of the membrane is the Monge gauge that specifies the location of the membrane with the coordinates $(\mathbf{r},h(\mathbf{r}))$ where $\mathbf{r}=(x,y)$. In the limit of small height fluctuations, the energy of a free bilayer, in the absence of external perturbation, is (Safran 1994)

$$H_{\text{free}} = \int_A \mathrm{d}\mathbf{r}\left\{\frac{k_c}{2}\left[\nabla^2 h(\mathbf{r})\right]^2 + \frac{\gamma}{2}[\nabla h(\mathbf{r}]^2\right\}, \tag{3}$$

where we have assumed that the spontaneous curvature vanishes. Typically, the area A is a square with sides L periodic in both the x and y directions.

The dynamics of Helfrich membranes can be derived from the Stokes equations for interacting particles in an incompressible fluid. In the low Reynolds number regime relevant to the cellular environment (Purcell 1977), inertia can be neglected and the velocity for each particle is affected by the motion other particles through a nonlocal hydrodynamic tensor (Doi and Edwards 1986). By adding a random force and taking the continuum limit, the equation governing the dynamics of the membrane is given by (Granek 1997)

$$\frac{\partial h(\mathbf{r},t)}{\partial t} = \int_{-\infty}^{\infty} \mathrm{d}\mathbf{r}'\Lambda(\mathbf{r}-\mathbf{r}')[F(h(\mathbf{r}',t),t) + \zeta(\mathbf{r}',t)], \tag{4}$$

where $\Lambda(\mathbf{r}-\mathbf{r}') = 1/8\pi\eta|\mathbf{r}-\mathbf{r}'|$ is the diagonal part of the Oseen tensor (Doi and Edwards 1986), η the viscosity of the surrounding fluid, $F(h(\mathbf{r},t),t) = -\delta H/\delta h(\mathbf{r},t)$ the force per unit area on the membrane and $\zeta(\mathbf{r},t)$ is a random force from either a thermal or non-thermal source. For complete generality, we allow for interactions through additional terms H_{int} in the Hamiltonian

$$H = H_{\text{free}} + H_{\text{int}}, \tag{5}$$

leading to a force per area

$$\begin{aligned} F(h(\mathbf{r},t),t) &= -\frac{\delta H_{\text{free}}}{\delta h(\mathbf{r},t)} - \frac{\delta H_{\text{int}}}{\delta h(\mathbf{r},t)} \\ &\equiv F_{\text{free}}(h(\mathbf{r},t),t) + F_{\text{int}}(h(\mathbf{r},t),t). \end{aligned} \tag{6}$$

Often, the random fluctuations $\zeta(\mathbf{r},t)$ are purely thermal in nature. In this case, we have Gaussian white noise with the moments of $\zeta(\mathbf{r},t)$ specified by the fluctuation–dissipation theorem (Doi and Edwards 1986). Whether the random forces are thermal or not, once their moments are specified, the above equations completely determine the time evolution of the system.

Although it is possible to handle Helfrich theory analytically in certain circumstances as mentioned in the introduction, quantitative studies of lipid bilayer

dynamics in the presence of general potentials in complex geometries are sometimes necessary. To achieve this goal, we require simulations of the membrane that are computationally efficient. Working in Fourier space is the solution and it has various other advantages that we discuss below.

We first consider the simplest case $H_{\text{int}}=0$ representing the free bilayer. In Fourier space, the Hamiltonian in Eq. 3 becomes

$$H_{\text{free}}=\frac{1}{2L^2}\sum_{\mathbf{q}}\left(k_c q^4+\gamma q^2\right)\left|h_{\mathbf{q}}\right|^2, \tag{7}$$

while the equation of motion in Eq. 4 is

$$\frac{\partial h_{\mathbf{q}}(t)}{\partial t}=-\omega_{\mathbf{q}}h_{\mathbf{q}}(t)+\Lambda_{\mathbf{q}}\zeta_{\mathbf{q}}(t) \tag{8}$$

with relaxation frequencies

$$\omega_{\mathbf{q}}=\frac{k_c q^3+\gamma q}{4\eta}. \tag{9}$$

In the free membrane, time evolution depends only on the single mode $h_{\mathbf{q}}$ and all equations are decoupled. Equation 8 is identical in form to that of an Ornstein-Uhlenbeck process (van Kampen 1992) and the exact solutions for all moments of $h_{\mathbf{q}}$ can be found (Brown 2003).

In the general case of a bilayer in an arbitrary potential, the equations of motion are

$$\frac{\partial h_{\mathbf{q}}(t)}{\partial t}=\Lambda_{\mathbf{q}}\left\{F_{\mathbf{q}}[h(\mathbf{r},t)]+\zeta_{\mathbf{q}}(t)\right\}, \tag{10}$$

where $F_{\mathbf{q}}=F_{\mathbf{q}}^{\text{free}}+F_{\mathbf{q}}^{\text{int}}$ is the Fourier transform of the force on the membrane in Eq. 6. In general, $F_{\mathbf{q}}$ is a functional of the height $h(\mathbf{r},t)$ and therefore depends on all the amplitudes $\{h_{\mathbf{q}}\}$. The set of equations represented by Eq. 1 then becomes coupled between modes and cannot in general be handled analytically except in some cases where the forces are harmonic (Granek and Klafter 2001; Lin and Brown 2004b). The only general method of quantitative analysis is therefore simulation.

The membrane is evolved forward in time (Lin and Brown 2004a) based on the principles of standard Brownian dynamics (Ermak and McCammon 1978). Although the basic idea is the same, we choose to evolve the Fourier modes since the convolution in Eq. 4 is more computationally expensive than performing a Fourier transform and using Eq. 10. In addition, it becomes straightforward to coarse grain over microscopic details by employing a cutoff for short wavelengths or, equivalently, large wave vectors.

We first integrate Eq. 10 from t to $t+\Delta t$

$$\begin{aligned} h_q(t+\Delta t)&=h_q(t)+\Lambda_q F_q(t)\Delta t+R_q(\Delta t),\\ R_q(\Delta t)&\equiv\Lambda_q\int_t^{t+\Delta t}\mathrm{d}t'\zeta_q(t'), \end{aligned} \tag{11}$$

where Δt is small enough that $F_{\mathbf{q}}[h(\mathbf{r},t)]$ is approximately constant over that time interval. For the purposes of simulation, the membrane must be discretized with lattice spacing chosen to be the desired short wavelength cutoff. The FSBD simulation method proceeds as follows:

1. Compute $h_{\mathbf{q}}$ from the current configuration $h(\mathbf{r})$ to calculate $F_{\mathbf{q}}^{\text{free}}$.
2. Using the current configuration $h(\mathbf{r})$, evaluate in position space the force due to the interactions $F_{\text{int}}(\mathbf{r})=-\delta H_{\text{int}}/\delta h(\mathbf{r})$ and compute the Fourier transform to obtain $F_{\mathbf{q}}^{\text{int}}$.
3. Pick $R_{\mathbf{q}}(\Delta t)$ from the appropriate distributions determined by the moments of the random force $\zeta_{\mathbf{q}}(t)$.
4. Compute $h_{\mathbf{q}}(t+\Delta t)$ using Eq. 11 and compute the inverse Fourier transform to obtain $h(\mathbf{r})$ for use in the next iteration. For the thermal case, $R_{\mathbf{q}}(\Delta t)$ are numbers drawn from Gaussian distributions with widths determined by the fluctuation–dissipation theorem. If $\zeta_{\mathbf{q}}(t)$ is non-thermal, then $R_{\mathbf{q}}(\Delta t)$ is computed from the moments that define the random force.

The above algorithm outlines the FSBD method for simulating lipid bilayers with Helfrich elastic energy and arbitrary interactions. In the following sections, we explore several applications of FSBD that include protein mobility on the red blood cell, membranes adhered to supported bilayers and non-thermal forces due to the pumping action of proteins embedded in the bilayer.

Applications

Protein mobility on the red blood cell

In the red blood cell, the lateral motion of band 3 protein on the cell surface has been shown to differ (Cherry 1979; Koppel et al. 1981; Schindler et al. 1980; Sheetz 1983; Sheetz et al. 1980) from the predictions of free diffusion in a two-dimensional fluid (Saffman and Delbruck 1975; Singer and Nicolson 1972). Studies of the diffusive behavior of band 3 protein embedded in the red blood cell membrane have shown that the macroscopic diffusion constant observed over long length scales (microns) is smaller than the microscopic diffusion constant observed over short length scales (<100 nm; Corbett et al. 1994; Edidin et al. 1991; Kusumi and Sako 1996; Tomishige et al. 1998; Tsuji et al. 1988; Tsuji and Ohnishi 1986). Qualitatively, this behavior is understood. Steric interaction between band 3 and the cytoskeleton is known to hinder the motion of the protein (see Fig. 2; Kusumi et al. 1993; Sheetz 1983). The cytoskeleton of the red blood cell is made of roughly triangular corrals composed of spectrin filaments (Byers and Branton 1985; Liu et al. 1987) pinned to the bilayer at discrete points (Jamney 1995; Luna and Hitt 1992; Sackmann 1995a; Steck 1989). The cytoplasmic domain of band 3 bumps into this structure and diffusive motion is hindered.

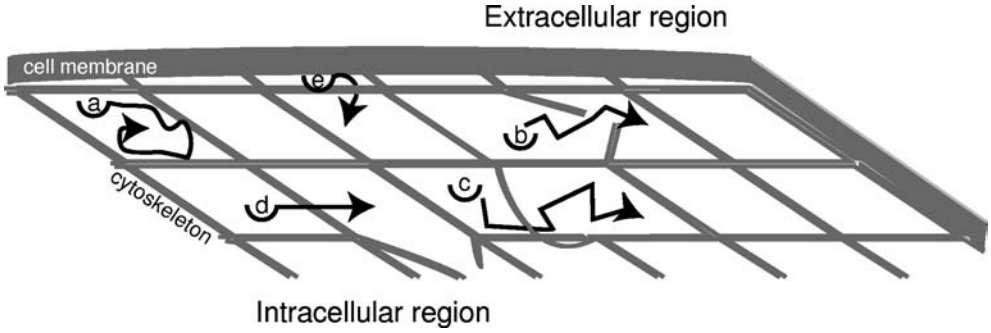

Fig. 2 Schematic illustration of the behavior of transmembrane proteins in the red blood cell. The cytoskeleton immediately below the membrane hinders protein transport by confining the protein temporarily to a localized corral (**a**). Jumps from one corral to another occur slowly and have previously been postulated to result from dynamic reorganization of the cytoskeletal matrix, either by dissociation of spectrin tetramers (**b**) or by thermal fluctuations in the shape of the cytoskeleton (**c**) or by infrequent crossing events where the protein is thermally kicked hard enough to force its way over a relatively static cytoskeleton (**d**). Our studies have considered the alternative possibility that shape fluctuations of the lipid bilayer may allow for corral hopping (**e**)

Since the protein does manage to explore the entire surface of the red blood cell, various theories have been proposed to explain how band 3 escapes confinement by the spectrin filaments as illustrated in Fig. 2. Previous theoretical studies have used simple, non-specific potential barriers at the corral boundary (Saxton 1995) or have assumed that rearrangements of the spectrin network are necessary for a protein to escape confinement (Brown et al. 2000; Leitner et al. 2000; Saxton 1989, 1990a, b). Although these mechanisms likely do play a role, we focus on thermal undulations of the bilayer as a means for promoting the passage of the protein over the cytoskeletal barrier (Brown 2003; Lin and Brown 2004a, b, 2005).

In our model, the height of the bilayer is influenced by both random thermal fluctuations and forces imposed by the attached spectrin filaments. We assume that the cytoskeleton lies in the $h(\mathbf{r})=0$ plane and only allows the protein to escape if the height of the bilayer at the corral edge exceeds the distance $h_0\sim$ 6 nm (Zhang et al. 2000) that the cytoplasmic domain of band 3 protrudes beneath the bilayer into the cell. In addition, the gap must persist for a sufficiently long period of time for the protein to diffuse over the barrier. The probability that $h(\mathbf{r},t)>h_0$ for times 0 and t can be approximated using the time correlation $\langle h(\mathbf{r},0)h(\mathbf{r},t)\rangle$. These statistical quantities allow us to estimate the macroscopic diffusion due to transverse bilayer undulations (Brown 2003; Lin and Brown 2004a, b, 2005).

Our first study of protein mobility in the context of thermal membrane undulations used free bilayers to estimate the macroscopic diffusion constant D_{macro} (Brown 2003). This model is analytically solvable as discussed previously and gives a macroscopic diffusion constant that is smaller than that obtained by experiment. A more realistic model, however, should incorporate the pinning between the membrane and the cytoskeleton at discrete points. We subsequently added localized, harmonic pinning interactions to the membrane (Lin and Brown 2004b). The form of the potential is given by

$$\mathscr{H}_{\mathrm{pin}}[h(\mathbf{r})]=\frac{\Gamma}{2}h^2(\mathbf{r})\sum_i\delta(\mathbf{r}-\mathbf{R}_i), \tag{12}$$

where Γ is a constant that determines the strength of the pinning and $\mathbf{R}_i$ are the locations of the pinning sites that are separated by the experimentally measured, median corral size $L_c\sim$ 110 nm (Tomishige et al. 1998). Since the potential is harmonic, analytical solutions can be found for the time correlation function by diagonalizing the appropriate matrices. In the final case, we retained the pinning sites and added repulsive interactions between the cytoskeleton and the bilayer through a hydration potential of the form (Lin and Brown 2004a, 2005)

$$\mathscr{H}_{\mathrm{rep}}[h(\mathbf{r})]=\epsilon\mathrm{e}^{-h(\mathbf{r})/\lambda}\sum_i\delta(a_ix+b_iy+c_i), \tag{13}$$

where ϵ and λ are constants and the repulsion is localized to the set of lines $a_ix+b_iy+c=0$. Since this interaction is non-harmonic, the FSBD simulation method is required to obtain quantitative results. Snapshots of the simulation for two different geometries of pinning sites are shown in Figs. 3 and 4.

Table 1 lists the calculated diffusion constants for the different models along with the experimental result. Note that the value of D_{macro} increases markedly when pinning is added. The reason is mainly because the system size L can then be increased beyond the size of the corrals L_c. For the free membrane, $L=L_c$ and the system size cannot be made larger because we would be adding unconstrained long-wavelength modes that are not present in the actual red blood cell. However, long-wavelength modes that are constrained by the pinning sites do exist in the real system. Examination of the Hamiltonian in Eq. 7 and the relaxation frequency in Eq. 9 shows that long-wavelength excitations dominate since they have lower energies and persist for longer times. In the square pinning geometry, the most important contribution comes from the $2L_c$ modes since they are the largest wavelength that satisfies the constraints of the pinning. For the triangular pinning, no particular mode is singled out but the longer wavelength

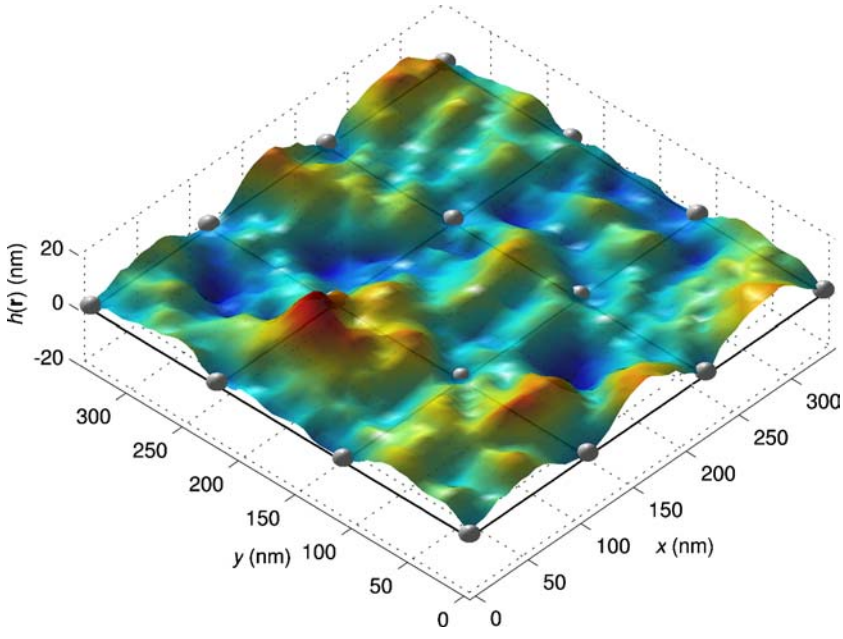

Fig. 3 Sample configuration from FSBD for a simulated red blood cell membrane with square pinning and cytoskeletal repulsion. The pinning sites are indicated by *spheres* and the repulsive interaction due to the spectrin is localized along the *black lines*. The *z*-axis is expanded to help visualize fluctuations in the membrane

modes do enhance the macroscopic diffusivity. Very long wavelengths are severely suppressed in both cases, allowing D_{macro} to converge as the simulation is made larger and larger (more and more corrals).

Adding the cytoskeletal repulsion decreases the macroscopic diffusion constant relative to the pinned-only model. Since the membrane is forced to be above the plane at the corral edges, the modes of wavelength $2L_c$ or larger are quenched in comparison to the system without repulsion. The suppression of these modes leads to a lower value of the diffusion constant by a factor of $\sim$2 or 3.

Although D_{macro} computed from our most detailed theory is $\sim$3 times larger than the experimental value, we cannot expect better agreement due to the simplified nature of our modeling. Our intention is not to quantitatively predict D_{macro}, but rather to ascertain whether thermal bilayer fluctuations are a feasible mechanism to allow the protein to escape from the corral. Our results conclusively show this assertion to be the case; thermal membrane undulations likely play a role in the mobility of band 3 on the surface of the red blood cell.

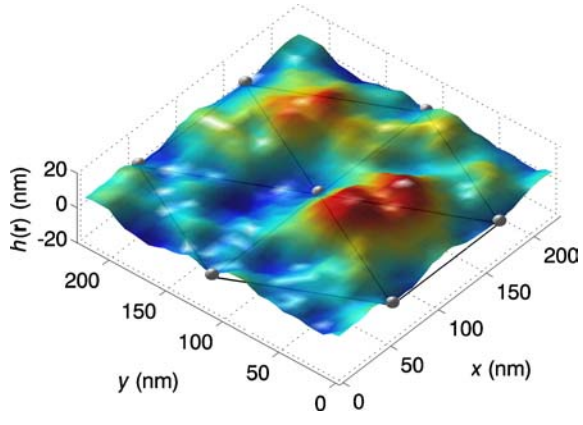

Fig. 4 Sample configuration from FSBD for a simulated red blood cell membrane with triangular pinning and cytoskeletal repulsion. The pinning sites are indicated by *spheres* and the repulsive interaction due to the spectrin is localized along the *black lines*. The *z*-axis is expanded to help visualize fluctuations in the membrane

Supported lipid bilayers

Lipid bilayers supported by solid substrates have become important tools for studying various membrane-related biophysical processes (Sackmann 1996). Supported membranes can be made to retain their fluidic properties (Sackmann and Tanaka 2000), making them useful for studying processes that involve the diffusion of components in the bilayer such as the formation of the immunological synapse (Grakoui et al. 1999).

Here, we focus on a recent study of supported intermembrane junctions (Kaizuka and Groves 2004). In these experiments, large unilamellar vesicles are ruptured over the supported bilayer and spontaneously adhere to the substrate at a random series of localized sites. The ruptured membrane is strongly pinned to the planar membrane on the support, although the nature of these adhesions is not well understood. The height of the upper membrane can subsequently be measured over a period of time using fluorescence interference contrast microscopy (Lambacher and Fromhertz 1996; Parthasarathy and Groves 2004). The resulting data are used to obtain the average height and the size of the fluctuations.

To model this system, we treat the upper bilayer as a Helfrich elastic sheet with two types of interactions with the supported bilayer underneath (L.C.-L. Lin and F.L.H. Brown, in preparation). The pinning between the two membranes is specified by the same interaction $\mathscr{H}_{\mathrm{pin}}[h(\mathbf{r})]$ as in Eq. 12. In addition, the upper membrane is repelled by the lower one through a hydration potential (Rand and Parsegian 1989). This repulsive interaction, specified by

Table 1 Results for the calculated macroscopic diffusion constant, D_{macro} ($\mu m^2\ s^{-1}$), for various models compared to the experimentally measured value (Tomishige et al. 1998)

	Square	Triangular
Pinned	7.0×10^{-2}	6.6×10^{-2}
Pinned and repulsive	3.4×10^{-2}	2.1×10^{-2}
Free	9.2×10^{-4}	
Experiment	6.6×10^{-3}	

The system size L for the free membrane model is median corral width L_c as measured by the experiment. For the pinned and repulsive cases, we have explored both a square geometry (see Fig. 3) and a triangular geometry (see Fig. 4). The results for these cases are converged in the limit of large system sizes

$$\mathscr{H}_{\text{rep}}[h(\mathbf{r})] = \epsilon e^{-h(\mathbf{r})/\lambda}, \tag{14}$$

is similar to Eq. 13 except that it is uniform over the entire plane. We have used FSBD to simulate the time evolution of the membrane and plot the average height of the membrane in Fig. 5. We employ a modified form of the hydrodynamic coupling in this simulation to account for the proximity of the planar support surface (L.C.-L. Lin and F.L.H. Brown, in preparation). This example demonstrates the flexibility of the FSBD simulation protocol to model bilayer systems in arbitrary geometries and with hydrodynamics incorporating non-infinite boundary conditions.

Active membranes

Thus far, we have only considered stochastic forces resulting from thermal fluctuations. Clearly, many biological processes of interest involve forces on the cell membrane of non-thermal origin. One example is the influence of membrane-bound proteins that turn energy from light or ATP into directed work. An elegant series of experiments have examined just this sort of process, but in a well-controlled environment. Prost and coworkers have studied membrane fluctuations induced by bacteriorhodopsin embedded in artificially constructed vesicles (Manneville et al. 1999, 2001). Bacteriorhodopsin exerts a force normal to the bilayer by pumping protons when activated by light. The experiments indicate a clear increase in the size of the height fluctuations when the pumps are activated. In addition, the size of the fluctuations decreases with increasing viscosity of solvent. Equilibrium averages in thermal systems can only depend on quantities specified in the Hamiltonian and not on the dynamical constants like the viscosity. These results clearly indicate that non-thermal effects in the system are being observed.

A number of theories have been proposed to explain various aspects of these experiments (Manneville et al. 2001; Prost and Bruinsma 1996; Prost et al. 1998; Ramaswamy et al. 1999, 2000). Recently, the viscosity dependence has been captured in a model by Gov (2004) where a set of uniformly distributed pumps change their state with a characteristic time constant τ. We have extended this model in several ways and used FSBD to verify our analytical results (L.C.-L. Lin et al., submitted). This application illustrates the utility of the FSBD method for explicitly time-dependent forces acting on the membrane surface.

In our model, the equations of motion are the same as in Eq. 8 except with $\zeta_{\mathbf{q}}(t)$ representing the fluctuating force exerted by the pumps. The moments and time-correlations of this force determine the size of the height fluctuations of the membrane. We have thus reduced bacteriorhodopsin to a point-like particle in our continuum simulation. While this level of description would be laughable for questions related to detailed protein dynamics, we find that we are able to reproduce various aspects of experiment with this picture. This has important implications for our understanding of the nature of coupling between protein and membrane and,

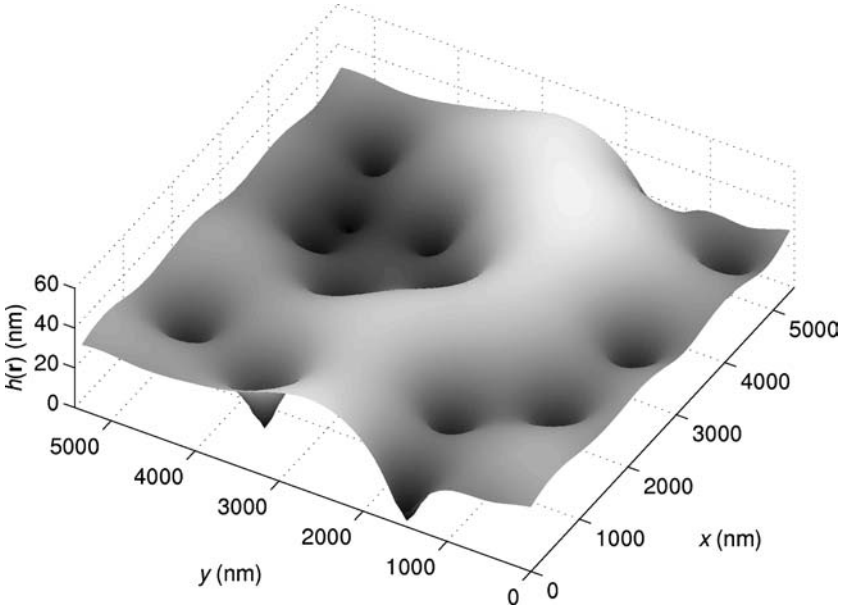

Fig. 5 Plot of the average height $\langle h(\mathbf{r})\rangle$ obtained by using FSBD for a membrane that contains pinning at multiple adhesion sites as well as a uniform repulsive interaction at the $h(\mathbf{r}) = 0$ plane. The potentials used in this system are intended to mimic that of a membrane pinned to a supported bilayer. Pinning sites were taken directly from experimental observation (adapted from Kaizuka and Groves 2004)

more generally, the gross effects of non-thermal energetics in the cellular environment.

The mean square height averaged over all positions $\mathbf{r}$ can be solved explicitly to give

$$\langle h^2 \rangle_{\mathbf{r}} = \frac{1}{L^2} \sum_{\mathbf{q}} \Lambda_{\mathbf{q}}^2 \lim_{t \to \infty} \int_0^t ds_1 \int_0^t ds_2 \langle \zeta_{\mathbf{q}}(s_1) \zeta_{-\mathbf{q}}(s_2) \rangle \, e^{\omega_{\mathbf{q}}(s_1+s_2-2t)}$$

The physics of the system is in the specification of the time correlation function of the stochastic forces.

In the model of Gov (2004), the proteins are distributed uniformly with a density n. Each protein exerts a time-dependent force $F(t)$ with moments given by $\langle F(t) \rangle = 0$ and the time correlation

$$\langle F(0)F(t) \rangle \sim F^2 e^{-t/\tau}. \tag{16}$$

We have chosen to use an equivalent model where the protein cycles with rate constant $k = 1/\tau$ between pushing up with force $+F$, pushing down with force $-F$ or off with zero force. The states are illustrated below in the state diagram:

$$\text{UP} \underset{k}{\overset{k}{\rightleftarrows}} \text{OFF} \underset{k}{\overset{k}{\rightleftarrows}} \text{DOWN}. \tag{17}$$

Although we take the on and off rates here to be equal, it is straightforward to allow different rates (L.C.-L. Lin et al., submitted).

There are several advantages to this model. It is easy to extend, as we will show below, and is straightforward to simulate using FSBD. In addition, this model allows for lattice sites on the membrane to be left empty thereby allowing for a non-uniform density. Consequently, we

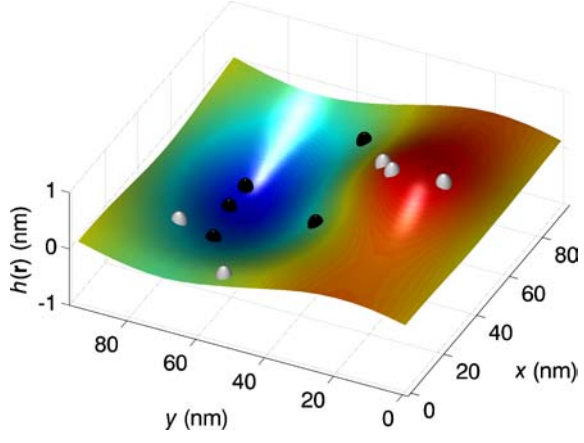

Fig. 6 Plot of the average height $\langle h(\mathbf{r}) \rangle$ obtained from FSBD for a system intended to represent a bilayer with embedded bacteriorhodopsin protein. Forces are exerted on the membrane when light induces proton pumping by the proteins. These forces turn on and off randomly according to a rate constant determined by the duration of the pumping cycle. Experimentally, about half of the bacteriorhodopsin pumps in the upward direction and the other half in the downward direction. In this simulation, five proteins push up (*white*) and five proteins push down (*black*). The proteins are static and initially randomly distributed

denote an average over all possible configurations of the proteins with a bar. The scaling behavior for this model is $\overline{\langle h^2 \rangle}_{\mathbf{r}} \sim F^2 n \tau L^3 / k_c \eta$ for $\gamma = 0$ and $\overline{\langle h^2 \rangle}_{\mathbf{r}} \sim F^2 n \tau L / \gamma \eta$ for $\gamma \neq 0$. Since the vesicles are of the order of tens of microns in diameter, we have taken the limit of a large system size L. Note that the fluctuations decrease with increasing viscosity as seen in the experiments.

Although this model reproduces some of the key features of the experiments, we note that bacteriorhodopsin is a unidirectional pump that is only capable of exerting a force in one direction. In the experiments, approximately half the population is embedded in the membrane in one direction while the rest is embedded in the other direction. The model above is therefore extended by incorporating two types of proteins with the state diagrams:

$$\text{OFF} \underset{k}{\overset{k}{\rightleftarrows}} \text{UP} \tag{18}$$

and

$$\text{OFF} \underset{k}{\overset{k}{\rightleftarrows}} \text{DOWN}. \tag{19}$$

Again, the model can be extended by making the on and off rates different if desired (L.C.-L. Lin et al., submitted), but we allow them to be the same for simplicity.

Although the mean square height can be solved analytically, we discuss briefly how to perform the FSBD simulation. The algorithm is the same as for thermal case except for the handling of the random force. At every time step Δt, each protein is given a probability $k\Delta t$ of switching between the on and off states. Depending on the state, the pump will either do nothing or exert a force of $\pm F$ during that time step. A plot of the average height of the membrane obtained from the simulation for a particular random distribution of proteins is shown in Fig. 6.

Proceeding analytically, the force correlation for each protein in this model is given by

$$\langle F(0)F(t) \rangle \sim F^2 \left(1 + e^{-2kt}\right). \tag{20}$$

However, the correlation between proteins at different sites does not vanish and is proportional to a time-independent constant F^2. Once these factors are taken into account, the solution for the mean square height is $\overline{\langle h^2 \rangle}_{\mathbf{r}} \sim F^2 n L^6 / k_c^2$ for $\gamma = 0$ and $\overline{\langle h^2 \rangle}_{\mathbf{r}} \sim F^2 n L^2 / \gamma^2$ for $\gamma \neq 0$. These results are summarized in Table 2.

Interestingly, the dependence on both the viscosity and τ disappear. Since the small $\mathbf{q}$ modes are the most important, we define a timescale for membrane relaxation $\tau_m = 1/\omega_{\mathbf{q}0}$ with $\mathbf{q}_0$ representing the longest wavelength mode. In the large L limit, τ_m becomes very large in comparison to τ and the pumps are switching rapidly between the on and off states relative to the membrane relaxation time. As a result, each protein essentially exerts a constant average force on the membrane and the resulting configuration is simply a static balance between this constant force and the elastic bending energy.

Table 2 Summary of the results for the scaling of the mean square height displacement $\overline{\langle h^2 \rangle}_{\mathbf{r}}$ for static and diffusing proteins in the limit of large L

	3 state ($\gamma = 0$)	3 state ($\gamma \neq 0$)	2 state ($\gamma = 0$)	2 state ($\gamma \neq 0$)
Static	$F^2 n\tau\ L^3/\kappa\eta$	$F^2 n\tau\ L/\gamma\eta$	$F^2 nL^6/\kappa^2$	$F^2 nL^2/\gamma^2$
Diffusing	$F^2 n\tau\ L^3/\kappa\eta$	$F^2 n\tau\ L/\gamma\eta$	$F^2\ nL^5/D\kappa\eta$	$F^2\ nL^2/\gamma^2$

The bar in the mean square height dispacement indicates an average over initial distributions while the subscript indicates an average over all positions $\mathbf{r}$. For the more realistic model with two protein types, the dependence on the viscosity η disappears except for the tensionless membrane with diffusing proteins

Therefore, neither τ_m, which contains η, nor τ affects the mean square height. This observation is contrasted with the model containing three-state proteins where the pump can switch between positive and negative values with zero average force. In that case, there is no static balance of forces and the membrane can relax. Both η and τ play a role since the rate at which the force switches signs compared to the rate of membrane relaxation determines the size of the height fluctuations.

To make the model more realistic, we allow the proteins to diffuse in the plane of the membrane. The force correlation now depends on the position and contains an additional factor

$$\langle F(0,0)F(\mathbf{r},t)\rangle \sim \frac{\mathrm{e}^{-r^2/4Dt}}{4Dt}. \tag{21}$$

In the large L limit, the results are $\overline{\langle h^2 \rangle}_{\mathbf{r}} \sim F^2 nL^5/D\kappa\eta$ for $\gamma = 0$ and $\overline{\langle h^2 \rangle}_{\mathbf{r}} \sim F^2 nL^2/\gamma^2$ for $\gamma \neq 0$. As in the static case, the timescale for switching between pump states is rapid compared to τ_m. The diffusion timescale $\tau_D = 1/Dq_0^2$ is also large compared to τ in the large L limit. The difference between the systems with and without tension is that $\tau_D \ll \tau_m$ for $\gamma = 0$ and $\tau_m \ll \tau_D$ for $\gamma \neq 0$. The viscosity dependence is only recovered in the tensionless case where diffusion occurs rapidly enough for the membrane to relax. When there is a finite tension, the diffusion is slow enough that the averages are over configurations containing a static balance of forces. The diffusion therefore is irrelevant and the result is the same as for the static case. The scaling dependence of the mean square height for diffusing proteins is summarized in Table 2. It should be noted, however, that various scaling behaviors can manifest themselves under different situations. The dependences on the various parameters depend on whether we are actually in the limit of large system sizes, whether the on and off rates are the same and what the values of the different constants are (L.C.-L. Lin et al., submitted).

Applications of molecular models

There are a number of questions for which continuum models are inappropriate. For instance, elastic constants such as the bending rigidity are simply inputs to a continuum model. Understanding what determines the bending rigidity requires an atomic or molecular model. Because atomic MD calculations of mesoscale membranes are computationally demanding, running the multiple simulations necessary to quantify trends is often computationally prohibitive. Coarse-grained models are useful for questions that require not only large systems, but also many systems or extensive sampling. We provide some examples of such questions, addressed using Monte Carlo simulations and our rigid and flexible models (see Fig. 1).

Model details

The single component version of our rigid model (Fig. 1c) is presented in detail in Brannigan and Brown (2004) and Brannigan et al. (2004), while the extension to multicomponent systems is presented in Brannigan and Brown (2005). Any two molecules interact through three potentials: a soft excluded volume repulsion between the distance of closest approach, a Lennard-Jones attraction between the points on the tail ends and an attractive alignment potential that depends on the relative orientations and the distance between the centers of mass. The model is constructed such that for flat homogeneous membranes at constant area, the average potential energy does not depend on the molecular length λ_i. For the heterogeneous systems, the same energetic parameters are used both for pairs of like and unlike molecules; all differences between species are reflected in rod length alone.

The five-bead version of our flexible model (Fig. 1d) is presented in Brannigan et al. 2005. All beads interact through the repulsive component of a standard Lennard-Jones potential. Hydrophobic–hydrophobic and hydrophobic–interface pairs interact through the attractive component of a Lennard-Jones potential as well. Interface–interface pairs interact through a truncated $1/r^2$ potential. All bond lengths are constrained and there are no dihedral potentials. There is a bond angle potential that is minimized when the chains are straight.

Phase behavior

Like thin films and smectic liquid crystals (Cheng et al. 1988; Chou et al. 1998; deGennes and Prost 1993; Pindak et al. 1981), melting in lipid bilayers (Luzzati 1968; Luzzati and Husson 1962) proceeds by a multistep process. Although the gel mesophase of lipid bilayers has been identified with the hexatic mesophase of two-dimensional melting (Smith et al. 1988, 1990), it is unclear to what degree the phase behavior in such systems is governed by the same physics. While phase diagrams (nematic, smectic, isotropic, etc.) have been measured for numerous liquid crystal models (Allen 1993)

including models with dipole moments (Weis et al. 1992) and hence qualitatively similar to our own rigid model, fewer simulation studies have investigated melting within the smectic phase. Furthermore, the existing studies (Aoki and Yonezawa 1992; Zangi and Rice 2003) typically involve stacks of single layers, rather than one bilayer. Since experiments (Chao et al. 1996; Cheng et al. 1988; Geer et al. 1992) suggest that location within the lamellar stack affects phase behavior, one cannot simply map the behavior of smectics onto that of a single bilayer, even if the bilayer is composed of rigid molecules. As a liquid crystal like model for bilayers, our rigid model is well suited to studying the relationship between generic quasi two-dimensional systems and lipid bilayers. We summarize a study investigating the effect of molecular elongation on bilayer phase behavior, first presented in Brannigan et al. (2004).

Main melting transition

The melting transition temperature in rigid molecule bilayers at constant vanishing tension was determined using the average projected area per molecule Σ and compared among rods with lengths ranging from $\lambda = 1.25\sigma$ to $\lambda = 2\sigma$. As shown in Fig. 7a, the main melting temperature decreases with increasing λ but the melting area per molecule is independent of λ. Like many amphiphilic assemblies (deGennes and Prost 1993) the system is lyotropic (density changes drive melting). Because area per molecule increases with aspect ratio at a given temperature, longer molecules undergo the transition at lower temperatures. This trend deviates from that observed in experimental systems and simulations of chain amphiphiles. Main melting temperature increases with increasing chain length in saturated diacyl phosphatidylcholines (Schneider et al. 1984), single-chain surfactants (Boyd et al. 2000) and simulated amphiphilic monolayers (Stadler and Schmid 1999). In these cases, the attractive energy of a membrane depends on the number of hydrophobic monomers in the chains. Lengthening the chains increases attractive interactions, which decreases the effective system temperature and leads to ordering. In contrast, since we vary the molecular length without increasing energetic attraction in our rigid model, the primary effect of lipid lengthening is to increase the area per lipid (rotational entropy favors larger area per lipid for longer molecules).

Hopping regime

Two-dimensional fluids are expected to display linear diffusion at long times:

$$\left\langle \left| \vec{r}_{\parallel}(t) - \vec{r}_{\parallel}(0) \right|^2 \right\rangle = 4D_{\parallel} t, \tag{22}$$

where $D_{\parallel}$ is the diffusion constant in the xy plane and t the time. In experimental model membranes, $D_{\parallel} \sim 10^{-9}$ cm^2/sec (Sackmann 1995b). For coarse-grained models it is not possible to directly compare a measured diffusion constant with an experimental measurement. Instead, one can mandate that the two are equivalent, thus extracting a dimensional time step. In Monte Carlo simulations one must be especially careful when interpreting the diffusion constant. Here we present diffusion constants for systems with the same move class, in units of σ^2/τ_{MC}, where 1 τ_{MC} corresponds to an attempt to rotate and translate each lipid 100 times.

Equation 22 is a necessary but insufficient indicator for fluidity. Figure 8c shows the mean squared particle displacement for a system at $k_B T = 0.84\epsilon$; this linear plot represents an average over numerous starting times and all particles. The system temperature is colder than the main transition, and careful examination showed that the measured diffusion takes place via hopping among

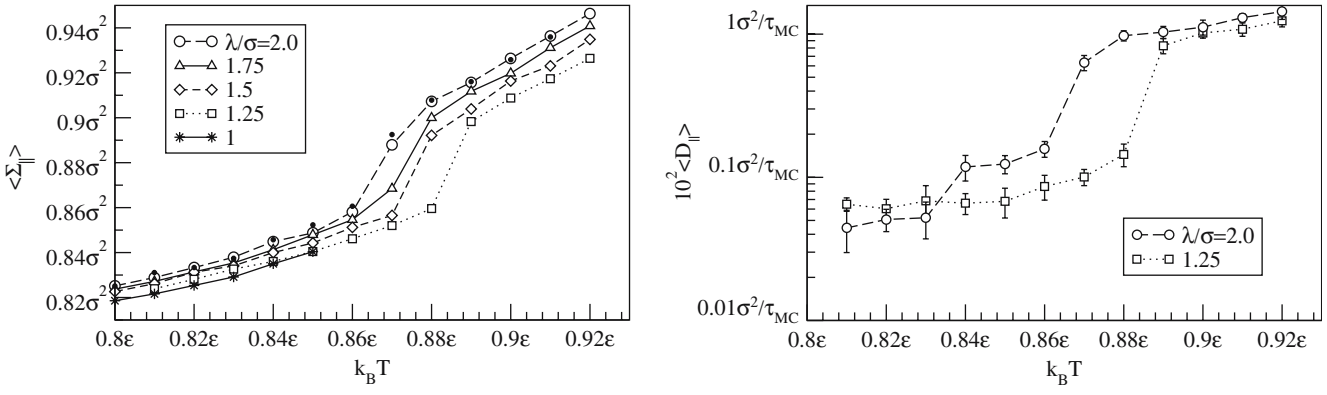

Fig. 7 The phase behavior in bilayers composed of rigid molecules was investigated both to identify a fluid regime and to test whether these systems exhibited multistep melting. The main melting transition was identified by plotting the average area per molecule as a function of temperature (*left*), for molecules with a range of aspect ratios. All systems at temperatures higher than the jump display liquid-like structure, and the size of the liquid regime decreases with aspect ratio. It is vanishingly small for the shortest molecule pictured. Diffusion constants as a function of temperature for the longest and shortest molecules with a main transition are shown on the *right*; in this plot two jumps are visible for $\lambda/\sigma = 2.0$. Closer examination indicates that molecules in the intermediate temperature regime are hopping among lattice sites (see Fig. 8). These figures originally appeared in Brannigan et al. (2004)

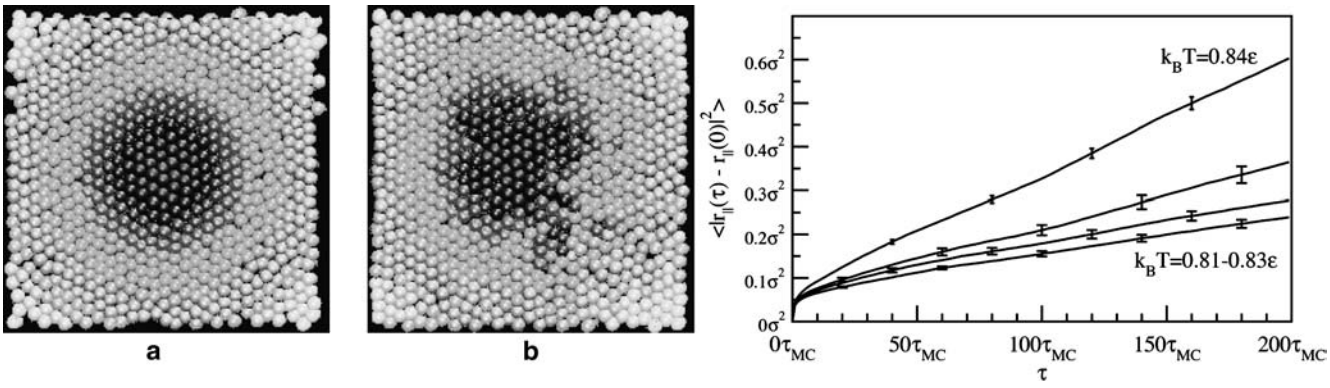

Fig. 8 In rigid molecule bilayers just below the melting temperature, molecules hop among triangular lattice sites. Configurations **a** and **b** are from the same system ($\lambda = 2\sigma$ and $k_BT = 0.84\epsilon$) but are separated by $800\tau_{MC}$. Each molecule in configuration **b** has retained its color from **a**. The lattice structure is basically unchanged between **a** and **b** but individual molecules have changed position. The hopping results in a linear form for the mean squared displacement (*right*), just as one observes in the liquid bilayers. The figure on the *right* originally appeared in Brannigan et al. (2004)

lattice sites. For instance, Fig. 8 shows an equilibrated configuration at $k_BT = 0.84\epsilon$, and the same system $800\tau_{MC}$ later. While the triangular lattice is basically maintained, individual molecules have switched lattice sites. Furthermore, the measured diffusion constants can be directly related to the hopping rate (Brannigan et al. 2004).

While merely obeying Eq. 22 does not indicate that a system is fluid, quantitative comparisons of diffusion constants do seem to be reasonable indicators of a transition. Using our rigid model we observed a jump in diffusion at the main transition temperature (Fig. 7b). For long molecules, we also observed a low temperature jump, which corresponds to a dramatic increase in the percentage of hopping molecules. As described in Brannigan et al. (2004) the diffusion constant (and the bond order) were used to designate a plausible solid–hexatic transition.

An aspect ratio–temperature phase diagram is shown in Fig. 9. The diagram suggests that when aspect ratio affects the excluded volume alone, both the solid–hexatic and hexatic–fluid transition temperatures decrease with increasing aspect ratio. Furthermore, no stable fluid phase is observed for aspect ratios $\lambda/\sigma < 1.25$.

Composition dependence of bending elasticity

Measurements of the fluctuation spectrum ($\langle |h_{\mathbf{q}}|^2 \rangle$) as a means to extract elastic constants from bilayer simulation have now become commonplace. Numerous simulation models (Brannigan and Brown 2004; Brannigan et al. 2005; Chiu et al. 2003; Cooke et al. 2005; Drouffe et al. 1991; Farago 2003; Goetz et al. 1999; Lindahl and Edholm 2000a; Loison et al. 2003; Marrink and Mark 2001; Stevens 2004) have verified that the Helfrich Hamiltonian describes fluctuations at wavelengths longer than the bilayer thickness. Although all have reported bending rigidities, the models and simulation conditions vary so much from study to study that it is difficult to infer precisely why, for instance, sphingomyelin (Chiu et al. 2003) is so much stiffer than glyceroolmonoolein (Marrink and Mark 2001) and dipalmitoylphosphatidylcholine (Lindahl and Edholm 2000a). Relatively few studies (Brannigan and Brown 2005; Brannigan et al. 2004, 2005; Illya et al. 2005; Imparato et al. 2005) have quantified how controlled changes in molecular architecture affect bilayer bending elasticity. Simplified molecular models are especially appropriate for understanding the influence of gross molecular properties, such as shape, chain length and flexibility.

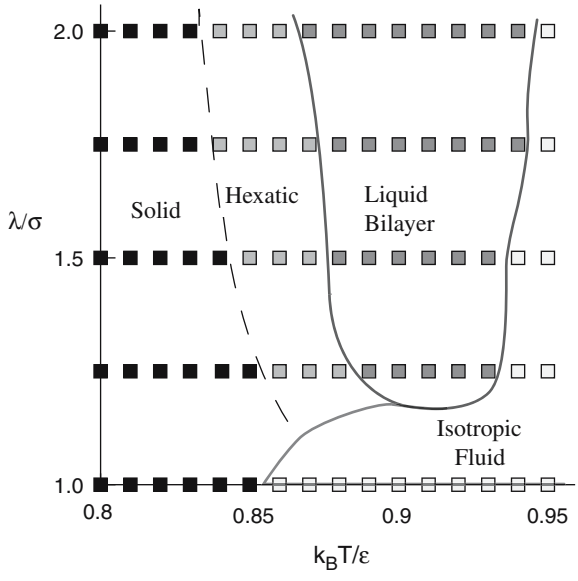

Fig. 9 Our rigid model is sufficiently simple that a phase diagram could be measured for a range of aspect ratios and temperatures: *squares* represent data points. Bilayers swell noticeably across the hexatic–liquid boundary, while the solid–hexatic boundary represents an increase in molecular hopping. The hexatic and liquid phases disappear as the molecules become more spherical. This figure originally appeared in Brannigan et al. (2004)

Thickness and heterogeneity

On dimensional grounds alone one can relate the bending rigidity k_c to the compressibility modulus k_A and the membrane thickness d, according to $k_c = k_A\, d^2/b$, where b is a dimensionless constant. Various theories have been put forth regarding the calculation of b. Continuum elastic theory suggests that b ranges from 4 to 48, depending on the stress profile (Bloom et al. 1991; Brannigan and Brown 2005; Evans 1974) and whether the leaflets are bound or unbound. A calculation that treats each leaflet as a polymer brush results in $b = 24$ (Rawicz et al. 2000).

Our rigid model is well suited to test scaling with thickness, because increasing the aspect ratio does not significantly alter the effective temperature. Bending rigidities for our rigid model at a range of aspect ratios (constant area and constant tension) are shown in Fig. 10a. The curve is a fit to the form $k_c = k_A\,(d - \Delta_d)^2/b$ and describes the data well. In heterogeneous systems, however, the situation is more complicated. Figure 10b shows the bending rigidity for a mixture of long and short molecules. Although the average membrane thickness is a monotonic function of composition, the bending rigidity is not. Instead the bending rigidity is fit to a function that includes an interaction term (Brannigan and Brown 2005). We note that a simultaneous publication (Imparato et al. 2005) using a solvated flexible model reported similar behavior.

Tail flexibility

Comparison between our rigid and flexible models allows some insight into the role of tail flexibility in determining bending elasticity. Measured bending rigidities for our flexible model are shown in Fig. 11; they are significantly lower than those reported for even the thin or heterogeneous rigid-molecule membranes. Unsurprisingly, the bending rigidity increases with the molecular rigidity. The difference between our rigid and flexible models are clearly seen in the elastic ratio b introduced above. Typical values (Sackmann 1995a) for k_A of one component phospholipid bilayers range from 60 to 270 mJ/m^2, and both the rigid and flexible models fell within this range. Both k_A and the thickness d are comparable for the two models, but we measured $b \sim 4$ (Brannigan et al. 2004) for the rigid model and $b \sim 60$ (Brannigan et al. 2005) for the flexible model. The difference lies, presumably, in the way stress is distributed throughout the membrane and/or the additional degrees of freedom granted a flexible molecule.

Even though simulations are run under conditions of vanishing surface tension, lipid bilayers are three-dimensional structures, and stress is not distributed evenly through the height of the membrane. In solvated bilayer systems, the hydrophilic heads and the hydrocarbon groups in the core of the membrane exert a positive pressure (negative tension) that is balanced by a positive tension localized at the hydrocarbon–water interface (Ben-Shaul 1995). One clear success of our flexible model is that it reproduces this behavior, as shown in Fig. 12, making it highly suitable for studies of bilayer deformations. The stress profiles agree qualitatively with those obtained from fully atomic models (Lindahl and Edholm 2000b) and nearly quantitatively with those obtained from solvated membranes also composed of five bead chains (Goetz and Lipowsky 1998). The peaks of high positive tension correspond to the positions of the interface beads, indicating that these beads are holding the bilayer together against the lateral repulsions of polar heads and the third and fourth beads. Furthermore, the tension due only to the interactions among interface beads is quite consistent with theoretical estimates of the interfacial tension in lipid bilayers (Brannigan et al. 2005). In short, the flexible model for lipids presented in Brannigan et al. (2005) passes at least as many tests (self-assembly, k_c, k_A, stress

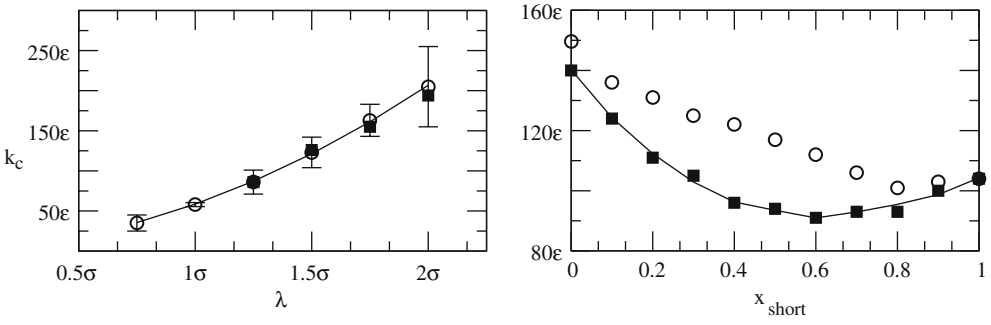

Fig. 10 In homogeneous systems composed of rigid molecules (*left*), the bending rigidity k_c is a simple function of molecular length λ and does not depend significantly on ensemble. Data taken at constant area (*circles*) and constant tension (*squares*) fall within error bars. The *curve*, predicted by elasticity theory, represents $k_c = k_A\,(2\lambda - \Delta_d)^2/b$ where k_A is the compressibility modulus and Δ_d and b are fit constants. In binary systems (*right*) composed of short and long molecules, there is a clear ensemble dependence. Here x_{short} is the mole fraction of short molecules in a binary simulation of rod lipids with $\lambda_l = 1.75\sigma$ and $\lambda_s = 1.25\sigma$. In the constant tension ensemble, the bending rigidity depends on both the average thickness and the number fraction of short molecules. The *curve* includes an interaction term, as described in Brannigan and Brown (2005). The *left* figure originally appeared in Brannigan et al. (2004), while the data on the *right* was presented in Brannigan and Brown (2005)

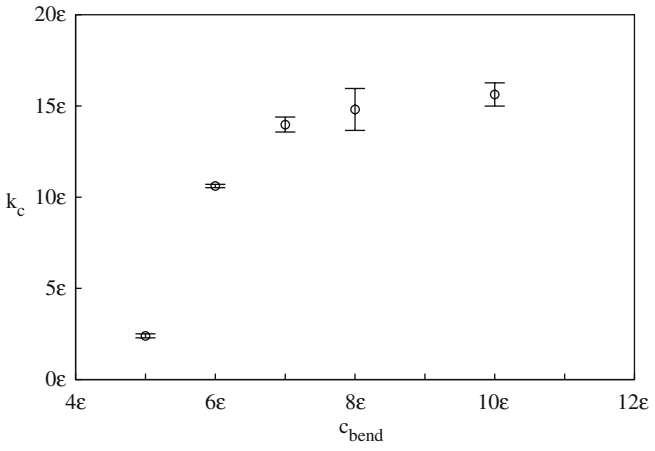

Fig. 11 Flexible molecules lead to flexible membranes, as shown in this figure. The bending rigidity k_c of a membrane composed of semiflexible molecules increases with the molecular bending coefficient, c_{bend}. Furthermore, these values for k_c are significantly lower than those resulting from the rigid model (Fig. 10) and are well within the range of biological relevance. This figure originally appeared in Brannigan et al. (2005)

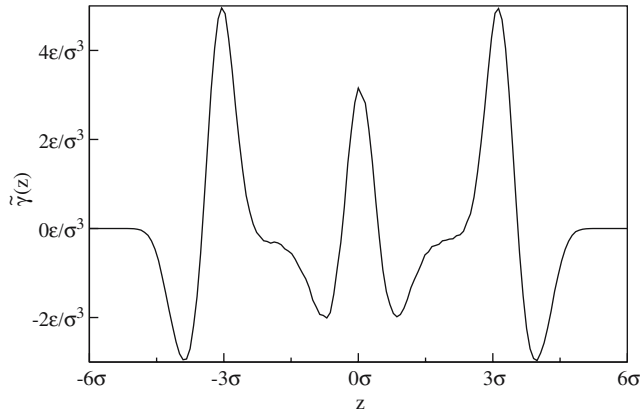

Fig. 12 The stress profile for our flexible molecule membranes is consistent with the profile measured in solvated models. In a real membrane, as in our model, repulsions among head groups result in the *outer valleys*, while repulsions among tails in the membrane core result in the *inner valleys*. These repulsions are balanced by a positive tension at the oil–water interfaces. In our model, this tension is due to attractions among interface beads, but the resulting stress profiles (compare for instance, Goetz and Lipowsky 1998) are equivalent. This figure originally appeared in Brannigan et al. (2005)

profile, interfacial tension) as do solvated models with a similar level of coarse-graining.

Inclusions

Inclusions embedded within the bilayer structure, such as proteins, are expected to deform the membranes in which they are embedded (Figs. 13, 14a). Experiments (Harroun et al. 1999; Planque et al. 1998; Weiss et al. 2003) can measure changes in, e.g., mean thickness upon peptide inclusion, but simulations provide a valuable tool for measuring the range and shape of the deformation. Analytical theories (Aranda-Espinoza et al. 1996; Dan et al. 1993, 1994; Fattal and Ben-Shaul 1993; Helfrich and Jakobsson 1990; Huang 1986; Kralchevsky et al. 1991; Marčelja 1976; May 2000; Netz 1997; Nielsen et al. 1998; Owicki and McConnell 1979; Partenskii and Jordan 2002) and experiments (de Planque and Killian 2003 and references therein) regarding inclusion deformations greatly outnumber simulation studies. Atomistic models (Jensen and Mouritsen 2004; Petrache et al. 2002) can be used for very high protein concentrations, but thus far only coarse-grained simulations (G. Brannigan and F.L. Brown, submitted; Nielsen et al. 2005; Venturoli et al. 2005) have observed the interesting behavior predicted for isolated proteins within the bilayer.

While coarse-grained models cannot necessarily be used to make quantitative predictions regarding the deformation profile, they are well suited for testing the multitude of available analytical theories. For instance, one persistent question in the theory of inclusion-induced deformations is whether the elastic constants that determine the deformation profile are the same as those that determine thermal fluctuations. We tested our simulations against an analytical theory that consistently

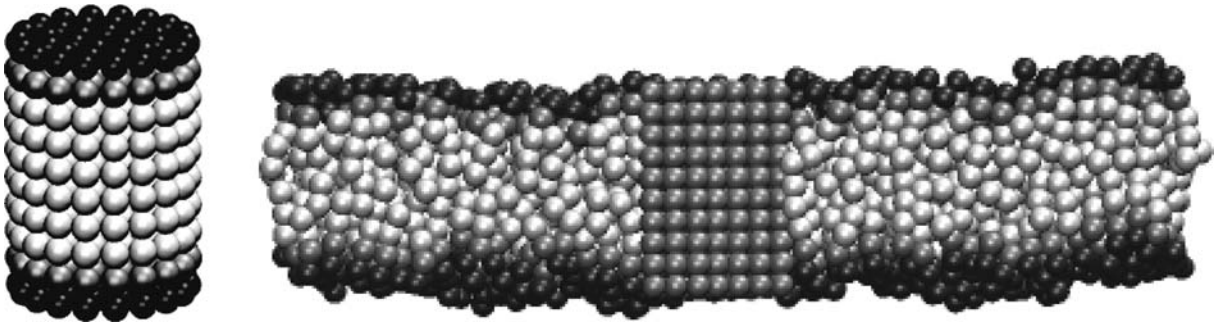

Fig. 13 In our model, inclusions (*left*) are constructed from the same chains used for lipid molecules, but the inclusions are completely rigid and all intramolecular distances are fixed. On the *right* is a cross-section of a membrane containing 3,214 lipid chains and one inclusion; the inclusion appears to straighten the adjacent lipids. These figures originally appeared in Brannigan and Brown (submitted)

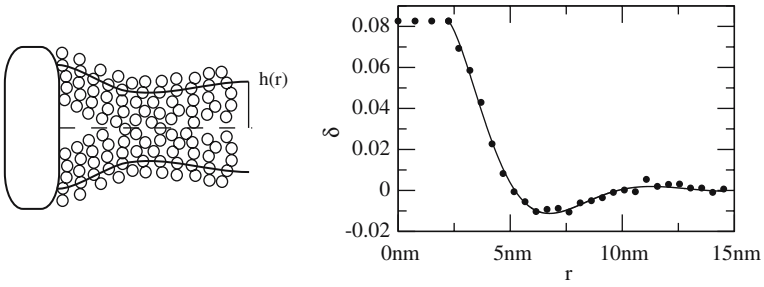

Fig. 14 An inclusion, such as a protein, can deform the surrounding membrane. As shown in the *cartoon on the left*, the inclusion straightens the surrounding lipids through both its length and its rigidity and may also weaken the bond between leaflets. Numerous analytical theories have been developed to describe the shape of the deformation. Upon inserting a rigid cylindrical protein into a bilayer composed of flexible molecules, we found that the deformation profile $\delta(r) = (h(r) - h_0)/h_0$ (*right*) was well fit by the theory of Aranda-Espinoza et al. (1996). This theory holds that the inclusion induces a bending deformation, and a preference for small curvatures results in the non-monotonic behavior shown in the plot. These figures originally appeared in Brannigan and Brown (submitted)

predicts both thickness fluctuations in an unperturbed bilayer and the thickness deformation profile in a perturbed bilayer (G. Brannigan and F.L. Brown, submitted). The analytical theory represents an extension of the works of Lipowsky and Grotehans (1994) and Aranda-Espinoza et al. (1996).

In principle, this test could be conducted using any model; in practice a sufficiently large box is needed with extensive sampling. Coarse-grained models are the only strategy presently feasible. The signature of the analytical model proposed by Aranda-Espinoza et al. (1996) is a non-monotonic deformation profile, but this is only expected for low protein concentrations. Venturoli et al. (2005), Nielsen et al. (2005) and ourselves (G. Brannigan and F.L. Brown, submitted) all observed non-monotonic behavior using coarse-grained models. The studies of Venturoli et al. and Nielsen et al., however, were more focused on protein tilting within the bilayer than testing analytical theories for the deformation profile, and the thickness fluctuations for an unperturbed bilayer were not reported. [Conversely, thickness fluctuations in atomistic bilayers (Chiu et al. 2003; Lindahl and Edholm 2000a; Marrink and Mark 2001) have been reported, but these models have not been used to study inclusions. However, as reported in Brannigan and Brown (submitted), the results of these atomistic simulations are consistent with our analytical theory for thickness fluctuations.]

Our simulation model for inclusions (Fig. 13) is similar to those used by Nielsen et al. (2005) and Venturoli et al. (2005). Inclusions are constructed from rigid chains with one head bead, one interface bead and three tail beads; if the surrounding lipids were completely straight, there would be no hydrophobic mismatch. The same interactions are used for, as an example, interface beads regardless of whether they are in lipid or inclusion molecules. Four concentric rings comprise the inclusion, and all intermolecular and intramolecular distances are held fixed.

Figure 14b depicts the thickness deformation profile $\delta(r) = (h(r) - h_0)/h_0$ at a distance r from the center of a cylindrical inclusion, where $h(r)$ is defined in Fig. 14a and h_0 is the average thickness of an unperturbed membrane. The profile is clearly non-monotonic, as originally predicted by Huang (1986). The curve is a fit to the theory of Aranda-Espinoza et al. (1996), as described in Brannigan and Brown (submitted), involving the following fit constants: the compressibility modulus k_A, the spontaneous curvature of a monolayer c_0 and the area derivative c'_0 of the spontaneous curvature evaluated at zero tension. These values were found to compare favorably (i.e., within error bars) to measurements via the thickness fluctuations and the stress profile.

There are two remarkable points to be made about this work. First, it is surprising that the continuum elastic theory of Aranda-Espinoza et al. (1996) is so successful given that the length scales considered are only several lipid diameters. Secondly, it is very encouraging to see that the deformations predicted by the solvent-free model employed by us agree not only with the analytical theory, but also with more complex simulations requiring the explicit simulation of solvent (Venturoli et al. 2005). The fact that our flexible model is able to capture not only thermal fluctuations correctly, but also more severe deformations of the bilayer indicates that it has quite general utility in modeling mesoscopic membrane behavior.

Conclusion

Relative to analytical theory, fully atomic simulation and solvated coarse-grained simulation, solvent-free simulation models for biomembranes are in their infancy. Still, these methods have clear practical appeal and have already begun to show compelling evidence of their suitability for use in mesoscale simulations. The models considered in detail here demonstrate that (1) it is possible and useful to extend dynamic Helfrich models to anharmonic potentials and complex geometries via Brownian dynamics simulation implemented in Fourier space and (2) fluid lipid bilayers may be stabilized by

effective pair potentials that obviate the need to explicitly simulate solvent in molecular level simulations.

Acknowledgments This work was supported in part by the NSF (MCB-0203221, CHE-0349196, CHE-0321368) and the donors of the American Chemical Society Petroleum Research Fund (PRF 42447-G7). F. B. is an Alfred P. Sloan Research Fellow. F. B. thanks the NSF for travel funds to participate in the "Biophysical Chemistry Meets Molecular Medicine" workshop.

References

Allen MP (1993) Simulations using hard particles. Philos Trans Phys Sci Eng 344:323–337

Aoki K, Yonezawa F (1992) Constant-pressure molecular-dynamics simulations of the crystal-smectic transition in systems of soft parallel spherocylinders. Phys Rev A 46:6541–6549

Aranda-Espinoza H, Berman A, Dan N, Pincus P, Safran SA (1996) Interaction between inclusions embedded in membranes. Biophys J 71:648–656

Ayton G, Voth GA (2002) Bridging microscopic and mesoscopic simulations of lipid bilayers. Biophys J 83:3357–3370

Ayton G, Bardenhagen SG, McMurty P, Sulsky D, Voth GA (2001) Interfacing continuum and molecular dynamics: an application to lipid bilayers. J Chem Phys 114:6913–6924

Bar-Ziv R, Menes R, Moses E, Safran SA (1995) Local unbinding of pinched membranes. Phys Rev Lett 75:3356–3359

Ben-Shaul A (1995) Molecular theory of chain packing. In: Lipowsky R, Sackmann E (eds) Structure and dynamics of membranes, vol 1. Elsevier, Amsterdam

Bloom M, Evans E, Mouritsen OG (1991) Physical-properties of the fluid lipid-bilayer component of cell membranes—a perspective. Q Rev Biophys 24:293–397

Boyd BJ, Drummond CJ, Krodkiewska I, Grieser F (2000) How chain length, headgroup polymerization, and anomeric configuration govern the thermotropic and lyotropic liquid crystalline phase behavior and the air–water interfacial adsorption of glucose-based surfactants. Langmuir 16:7359–7367

Brannigan G, Brown FLH (2004) Solvent-free simulations of fluid membrane bilayers. J Chem Phys 120:1059

Brannigan G, Brown FL (2005) Composition dependence of bilayer elasticity. J Chem Phys 122:074905

Brannigan G, Tamboli AC, Brown FLH (2004) The role of molecular shape in bilayer phase behavior and elasticity. J Chem Phys 121:3259–3271

Brannigan G, Philips PF, Brown FL (2005) Flexible lipid bilayers in implicit solvent. Phys Rev E 72:011915

Brochard F, Lennon JF (1975) Frequency spectrum of the flicker phenomenon in erythrocytes. J Phys (Paris) 36:1035–1047

Brown FLH (2003) Regulation of protein mobility via thermal membrane undulations. Biophys J 84:842–853

Brown FLH, Leitner DM, McCammon JA, Wilson KR (2000) Lateral diffusion of membrane proteins in the presence of static and dynamic corrals: suggestions for appropriate observables. Biophys J 78:2257–2269

Byers TJ, Branton D (1985) Visualization of the protein associations in the erythrocyte membrane skeleton. Proc Natl Acad Sci USA 82:6153–6157

Canham PB (1970) The minimum energy of bending as a possible explanation of the biconcave shape of the red blood cell. J Theor Biol 26:61–81

Chao C-Y, Chou C-F, Ho JT, Hui S, Jin A, Huang CC (1996) Nature of layer-by-layer freezing in free-standing 4o.8 films. Phys Rev Lett 77:2750–2753

Cheng M, Ho JT, Hui SW, Pindak R (1988) Observation of two-dimensional hexatic behavior in free-standing liquid crystal films. Phys Rev Lett 61:550–553

Cherry RJ (1979) Rotational and lateral diffusion of membrane proteins. Biochim Biophys Acta 559:289–327

Chiu SW, Jakobsson E, Mashl RJ, Scott HL (2002) Cholesterol-induced modifications in lipid bilayers: a simulation study. Biophys J 83:1842–1853

Chiu S, Vasudevan S, Jakobsson E, Mashl RJ, Scott HL (2003) Structure of sphingomyelin bilayers: a simulation study. Biophys J 85:3624–3635

Chou C-F, Jin AJ, Hui S, Huang CC, Ho JT (1998) Multiple-step melting in two-dimensional hexatic liquid-crystal films. Science 280:1424–1426

Cooke IR, Kremer K, Deserno M (2005) Tunable generic model for fluid bilayer membranes. Phys Rev E 72:011506

Corbett JD, Agre P, Palek J, Golan DE (1994) Differential control of band 3 lateral and rotational mobility in intact red cells. J Clin Invest 94:683–688

Dan N, Pincus P, Safran SA (1993) Membrane-induced interactions between inclusions. Langmuir 9:2768–2771

Dan N, Berman A, Pincus P, Safran SA (1994) Membrane-induced interactions between inclusions. J Phys II France 4:1713–1725

Deuling HJ, Helfrich W (1976) The curvature elasticity of fluid membranes: a catalogue of vesicle shapes. J Phys (Paris) 37:1335–1345

Dill KA, Bromberg S, Yue K, Fiebig KM, Yee DP, Thomas PD, Chan HS (1995) Principles of protein folding—a perspective from simple exact models. Protein Sci 4:561–602

Doi M, Edwards SF (1986) The theory of polymer dynamics. Clarendon Press, Oxford

Drouffe J-M, Maggs AC, Leibler S (1991) Computer simulations of self-assembled membranes. Science 254:1353–1356

Edidin M, Kuo SC, Sheetz MP (1991) Lateral movements of membrane glycoproteins restricted by dynamic cytoplasmic barriers. Science 254:1379–1382

Edwards L, Peng Y, Reggia JA (1998) Computational models for the formation of protocell structures. Artif Life 4:61–77

Ermak DL, McCammon JA (1978) Brownian dynamics with hydrodynamic interactions. J Chem Phys 69:1352–1360

Evans E (1974) Bending resistance and chemically induced moments in membrane bilayers. Biophys J 14:923–931

Evans E, Skalak R (1980) Mechanisms and thermodyanmics of biomembranes. CRC Press, Boca Raton

Farago O (2003) "Water-free" computer model for fluid bilayer membranes. J Chem Phys 119:596–605

Farago O (2004) Statistical mechanics of bilayer membrane with a fixed projected area. J Chem Phys 120:2934–2950

Fattal D, Ben-Shaul A (1993) A molecular model for lipid–protein interaction in membranes: the role of hydrophobic mismatch. Biophys J 65:1795–1809

Feig M, Brooks CL III (2004) Recent advances in the development and application of implicit solvent models in biomolecule simulations. Curr Opin Struct Biol 14:217–224

Feller SE (2000) Molecular dynamics simulations of lipid bilayers. Curr Opin Colloid Interface 5:217–223

Geer R, Stoebe T, Huang CC, Pindak R, Goodby J, Cheng M, Ho JT, Hui SW (1992) Liquid–hexatic phase transitions in single molecular layers of liquid-crystal films. Nature 355:152–154

deGennes P, Prost J (1993) The physics of liquid crystals, 2nd edn. Clarendon Press, Oxford

Gennis RB (1989) Biomembranes: molecular structure and function. Springer, Berlin Heidelberg New York

Goetz R, Lipowsky R (1998) Computer simulations of bilayer membranes: self assembly and interfacial tension. J Chem Phys 108:7397–7409

Goetz R, Gompper G, Lipowsky R (1999) Mobility and elasticity of self-assembled membranes. Phys Rev Lett 82:221–224

Gompper G, Kroll DM (1997) Network models of fluid, hexatic and polymerized membranes. J Phys Condens Matter 9:8795–8834

Gouliaev N, Nagle JF (1998a) Simulations of a single membrane between two walls using a Monte Carlo method. Phys Rev E 58:881–888

Gouliaev N, Nagle JF (1998b) Simulations of interacting membranes in the soft confinement regime. Phys Rev Lett 81:2610–2613

Gov N (2004) Membrane undulations driven by force fluctuations of active proteins. Phys Rev Lett 93:268104
Gov N, Safran SA (2004) Pinning of fluid membranes by periodic harmonic potentials. Phys Rev E 69:011101
Gov N, Zilman AG, Safran S (2003) Cytoskeleton confinement and tension of red blood cells. Phys Rev Lett 90:228101
Gov N, Zilman AG, Safran SA (2004) Hydrodynamics of confined membranes. Phys Rev E 70:011104
Gove PB (ed) (1970) Webster's seventh new collegiate dictionary. G. & C. Merriam, Springfield
Grakoui A, Bromley SK, Sumen C, Davis MM, Shaw AS, Allen PM, Dustin ML (1999) The immunological synapse: a molecular machine controlling t cell activation. Science 285:221–227
Granek R (1997) From semi-flexible polymers to membranes: anomalous diffusion and reptation. J Phys II (Paris) 7:1761–1788
Granek R, Klafter J (2001) Anomalous motion of membranes under a localized external potential. Europhys Lett 56:15–21
Groot RD, Rabone KL (2001) Mesoscopic simulation of cell membrane damage, morphology change and rupture by nonionic surfactants. Biophys J 81:725
Gruhn T, Lipowsky R (2005) Temperature dependence of vesicle adhesion. Phys Rev E 71:011903
Harries D, Ben-Shaul A (1997) Conformational chain statistics in a model lipid bilayer: comparison between mean field and Monte Carlo calculations. J Chem Phys 106:1609–1619
Harroun TA, Heller WT, Weiss T, Yang L, Huang HW (1999) Experimental evidence for hydrophobic matching and membrane-mediated interactions in lipid bilayers containing gramicidin. Biophys J 76:937–945
Helfrich W (1973) Elastic properties of lipid bilayers: theory and possible experiments. Z Naturforsch 28c:693–703
Helfrich W (1978) Steric interaction of fluid membranes in multilayer systems. Z Naturforsch 33a:305–315
Helfrich P, Jakobsson E (1990) Calculation of deformation energies and conformations in lipid membranes containing gramicidin channels. Biophys J 57:1075–1084
Holzöhner R, Schoen M (1999) Attractive forces between anisotropic inclusions in the membrane of a vesicle. Eur Phys J B 12:413–419
Huang H (1986) Deformation free energy of bilayer membrane and its effects on gramicidin channel lifetime. Biophys J 50:1061–1070
Illya G, Lipowsky R, Shillcock JC (2005) Effect of chain length and asymmetry on material properties of bilayer membranes. J Chem Phys 122:244901
Im W, Feig M, Brooks CL III (2003) An implicit membrane generalized born theory for the study of structure, stability and interactions of membrane proteins. Biophys J 85:2900–2918
Imparato A, Shillcock J, Lipowsky R (2005) Shape fluctuations and elastic properties of two-component bilayer membranes. Europhys Lett 69:650–656
Izvekov S, Voth GA (2005) A multi-scale coarse-graining method for biomolecular systems. J Phys Chem B 109:2469
Jamney P (1995) Cell membranes and the cytoskeleton. In: Structure and dynamics of membranes: part A. From cells to vesicles. Elsevier, Amsterdam, pp 805–849
Jensen MO, Mouritsen OG (2004) Lipids do influence protein function—the hydrophobic matching hypothesis revisited. Biochim Biophys Acta 1666:205–226
Kaizuka Y, Groves JT (2004) Structure and dynamics of supported intermembrane junctions. Biophys J 86:905–912
van Kampen NG (1992) Stochastic processes in physics and chemistry. North-Holland, Amsterdam, pp 63, 83, 220-221
Kohyama T, Kroll D, Gompper G (2003) Budding of crystalline domains in fluid membranes. Phys Rev E 68:061905
Kolinski A, Skolnick J (2004) Reduced models of proteins and their applications. Polymer 45:511–524
Koppel DE, Sheetz MP, Schindler M (1981) Matrix control of protein diffusion in biological membranes. Proc Natl Acad Sci USA 78:3576–3580
Kralchevsky P, Paunov V, Dekov ND, Nagayama K (1991) Stresses in lipid membranes and interactions between inclusions. J Chem Soc Faraday Trans 91:3415–3432
Kumar PS, Rao M (1998) Shape instabilities in the dynamics of a two-component fluid membrane. Phys Rev Lett 80:2489–2492
Kumar PS, Gompper G, Lipowsky R (2001) Budding dynamics of multicomponent membranes. Phys Rev Lett 86:3911–3914
Kusumi A, Sako Y (1996) Cell surface organization by the membrane skeleton. Curr Opin Cell Biol 8:566–574
Kusumi A, Sako Y, Yamamoto M (1993) Confined lateral diffusion of membrane receptors as studied by single particle tracking. Effects of calcium-induced differentiation in cultured epithelial cells. Biophys J 65:2021–2040
Lambacher A, Fromhertz P (1996) Fluorescence interference-contrast microscopy on oxidized silicon using a monomolecular dye layer. Appl Phys A 63:207–216
Laradji M (1999) Polymer adsorption on fluctuating surfaces. Europhys Lett 47:694–700
Laradji M (2002) Elasticity of polymer-anchored membranes. Europhys Lett 60:594–600
Laradji M (2004) A Monte Carlo study of fluctuating polymer-grafted membranes. J Chem Phys 121:1591–1600
Laradji M, Kumar PS (2004) Dynamics of domain growth in self-assembled fluid vesicles. Phys Rev Lett 93:198105
Leitner DM, Brown FLH, Wilson KR (2000) Regulation of protein mobility in cell membranes: a dynamic corral model. Biophys J 78:125–135
Lim HWG, Wortis M, Mukhopadhyay R (2002) Stomatocyte–discocyte–echinocyte sequence of the human red blood cell: evidence for the bilayer-couple hypothesis from membrane mechanics. Proc Natl Acad Sci 99:16766–16769
Lin LC-L, Brown FLH (2004a) Brownian dynamics in fourier space: membrane simulations over long length and time scales. Phys Rev Lett 93:256001
Lin LC-L, Brown FLH (2004b) Dynamics of pinned membranes with application to protein diffusion on the surface of red blood cells. Biophys J 86:764–780
Lin LC-L, Brown FLH (2005) Dynamic simulations of membranes with cytoskeletal interactions. Phys Rev E 72:011910
Lindahl E, Edholm O (2000a) Mesoscopic undulations and thickness fluctuations in lipid bilayers from molecular dynamics simulations. Biophys J 79:426–633
Lindahl E, Edholm O (2000b) Spatial and energetic-entropic decomposition of surface tension in lipid bilayers from molecular dynamics simulations. J Chem Phys 113:3882–3893
Lipowsky R (1991) The conformation of membranes. Nature 349:475–481
Lipowsky R, Grotehans S (1994) Renormalization of hydration forces by collective protrusion modes. Biophys Chem 49:27–37
Lipowsky R, Sackmann E (1995) Structure and dynamics of membranes. Elsevier, Amsterdam
Lipowsky R, Zielenska B (1989) Binding and unbinding of lipid membranes: a Monte Carlo study. Phys Rev Lett 62:1572–1575
Liu S, Derick L, Palek J (1987) Visualization of the hexagonal lattice in the erythrocyte membrane skeleton. J Cell Biol 104:527–536
Lodish H, Baltimore D, Berk A, Zipursky SL, Matsudaira P, Darnell J (1995) Molecular cell biology, 3rd edn. Scientific American Books, New York
Loison C, Mareschal M, Kremer K, Schmid F (2003) Thermal fluctuations in a lamellar phase of a binary amphiphile–solvent mixture: a molecular-dynamics study. J Chem Phys 119:13138–13148
Luna EJ, Hitt AL (1992) Cytoskeleton–plasma membrane interactions. Science 258:955–964
Luzzati V (1968) X-ray diffraction studies of lipid-water systems. In: Chapman D (ed) Biological membranes, vol 1. Academic, New York, pp 71–123
Luzzati V, Husson F (1962) Structure of liquid-crystalline phases of lipid water systems. J Cell Biol 12:207

Manneville J-B, Bassereau P, Levy D, Prost J (1999) Activity of transmembrane proteins induces magnification of shape fluctuations of lipid membranes. Phys Rev Lett 82:4356–4359
Manneville J-B, Bassereau P, Ramaswamy S, Prost J (2001) Active membrane fluctuations studied by micropipet aspiration. Phys Rev E 64:021908
Marčelja S (1976) Lipid-mediated protein interaction in membranes. Biochim Biophys Acta 455:1–7
Marrink SJ, Mark AE (2001) Effect of undulations on surface tension in simulated bilayers. J Phys Chem 105:6122–6127
Marrink S-J, Berkowitz M, Berendsen HJC (1993) Molecular dynamics simulation of a membrane/water interface: the ordering of water and its relation to the hydration force. Langmuir 9:3122–3131
Marrink S-J, Lindahl E, Edholm O, Mark AE (2001) Simulation of the spontaneous aggregation of phospholipids into bilayers. J Am Chem Soc 2001:8638–8639
Marrink S, de Vries A, Mark AE (2004) Coarse grained model for semiquantitative lipid simulations. J Phys Chem B 108:750–760
May S (2000) Theories on structural perturbations of lipid bilayers. Curr Opin Colloid Interface Sci 5:244–249
McWhirter JL, Ayton G, Voth GA (2004) Coupling field theory with mesoscopic dynamical simulations of multicomponent lipid bilayers. Biophys J 87:3242–3263
Miao L, Fourcade B, Wortis MRM, Zia RKP (1991) Equilibrium budding and vesiculation in the curvature model of fluid lipid vesicles. Phys Rev A 43:6843–6856
Miao L, Seifert U, Wortis M, Döbereiner H (1994) Budding transitions of fluid-bilayer vesicles: the effect of area-difference elasticity. Phys Rev E 49:5389–5407
Milner ST, Safran SA (1987) Dynamical fluctuations of droplet microemulsions and vesicles. Phys Rev A 36:4371–4379
Moore GE (1985) Cramming more components onto integrated circuits. Electronics 38:114–117
Morikawa R, Saito Y (1994) Hard rod and frustum model of two-dimensional vesicles. J Phys II 4:145
Mukhopadhyay R, Lim HWG, Wortis M (2002) Echinocyte shapes: bending, stretching, and shear determine spicule shape and spacing. Biophys J 82:1756–1772
Murtola T, Falck E, Patra M, Karttunen M, Vattulainen I (2004) Coarse-grained model for phospholipid/cholesterol bilayer. J Chem Phys 121:9156–9165
Nagle JF, Tristram-Nagle S (2000) Structure of lipid bilayers. Biochim Biophys Acta 1469:159–195
Netz RR (1997) Inclusions in fluctuating membranes: exact results. J Phys I France 7:833–852
Nielsen C, Goulian M, Andersen OS (1998) Energetics of inclusion-induced bilayer deformations. Biophys J 74:1966–1983
Nielsen SO, Ensing B, Ortiz V, Moore PB, Klein ML (2005) Lipid bilayer perturbations around a transmembrane nanotube: a coarse grain molecular dynamics study. Biophys J 88:3822–3828
Noguchi H (2002) Fusion and toroidal formation of vesicles by mechanical forces: a brownian dynamics simulation. J Chem Phys 117:8130–8137
Noguchi H (2003) Polyhedral vesicles: a brownian dynamics simulation. Phys Rev E 67:041901
Noguchi H, Gompper G (2004) Fluid vesicles with viscous membranes in shear flow. Phys Rev Lett 93:258102
Noguchi H, Takasu M (2001a) Fusion pathways of vesicles: a brownian dynamics simulation. J Chem Phys 115:9547–9551
Noguchi H, Takasu M (2001b) Self-assembly of amphiphiles into vesicles: a brownian dynamics simulation. Phys Rev E 64:041913
Noguchi H, Takasu M (2002a) Adhesion of nanoparticles to vesicles: a brownian dynamics simulation. Biophys J 83:299–308
Noguchi H, Takasu M (2002b) Structural changes of pulled vesicles: a brownian dynamics simulation. Phys Rev E 65:051907
Owicki J, McConnell HM (1979) Theory of protein–lipid and protein–protein interactions in bilayer membranes. Proc Natl Acad Sci 76:4750–4754
Partenskii MB, Jordan PC (2002) Membrane deformation and the elastic energy of insertion: perturbation of membrane elastic constants to due peptide insertion. J Chem Phys 117:10768–10776
Parthasarathy R, Groves JT (2004) Optical techniques for imaging membrane topography. Cell Biochem Biophys 41:391–414
Pastor RW (1994) Molecular-dynamics and Monte-Carlo simulations of lipid bilayers. Curr Opin Struct Biol 4:486–492
Petrache H, Zuckerman D, Sachs J, Killian J, Koeppe R, Woolf TB (2002) Hydrophobic matching mechanism investigated by molecular dynamics simulations. Langmuir 18:1340–1351
Pindak R, Moncton DE, Davey SC, Goodby JW (1981) X-ray observation of a stacked hexatic liquid-crystal *b* phase. Phys Rev Lett 46:1135
Pitman MC, Grossfield A, Suits F, Feller SE (2005) Role of cholesterol and polyunsaturated chains in lipid–protein interactions: molecular dynamics simulation of rhodopsin in a realistic membrane environment. J Am Chem Soc 127:4576–4577
de Planque M, Killian J (2003) Protein–lipid interactions studied with designed transmembrane peptides: role of hydrophobic matching and interfacial anchoring. Mol Membr Biol 20:271–284
Planque MRD, Greathouse D, Koeppe R, Schäfer H, Marsh D, Killian JA (1998) Influence of lipid/peptide hydrophobic mismatch on the thickness of diacylphosphatidylcholine bilayers: a ^{2}H-nmr and esr study using designed transmembrane α-helical peptides and gramicidin a. Biochemistry 37:9333–9345
Prost J, Bruinsma R (1996) Shape fluctuations of active membranes. Europhys Lett 33:321–326
Prost J, Manneville J-B, Bruinsma R (1998) Fluctuation-magnification of non-equilibrium membranes near a wall. Eur Phys J B 1:465–480
Purcell EM (1977) Life at low reynolds number. Am J Phys 45:3–10
Qi SY, Groves JT, Chakraborty AK (2001) Synaptic pattern formation during cellular recognition. Proc Natl Acad Sci USA 98:6548–6553
Ramaswamy S, Toner J, Prost J (1999) Nonequilibrium noise and instabilities in membranes with active pumps. Pramana J Phys 53:237–242
Ramaswamy S, Toner J, Prost J (2000) Nonequilibrium fluctuations, traveling waves, and instabilities in active membranes. Phys Rev Lett 84:3494–3497
Rand RP, Parsegian VA (1989) Hydration forces between phospholipid-bilayers. Biochim Biophys Acta 988:351–376
Rawicz W, Oldbrich K, McIntosh T, Needham D, Evans E (2000) Effect of chain length and unsaturation on elasticity of lipid bilayers. Biophys J 79:328–339
Rekvig L, Kranenburg M, Vreede J, Hafskjold B, Smit B (2003) Investigation of surfactant efficiency using dissipative particle dynamics. Langmuir 19:4897
Sackmann E (1995a) Biological membranes architecture and function. In: Structure and dynamics of membranes: part A. From cells to vesicles. Elsevier, Amsterdam, pp 1–62
Sackmann E (1995b) Physical basis of self-organization and function of membranes: physics of vesicles. In: Lipowsky R, Sackmann E (eds) Structure and dynamics of membranes, vol 1. Elsevier, Amsterdam
Sackmann E (1996) Supported membranes: scientific and practical applications. Science 271:43–48
Sackmann E, Tanaka M (2000) Supported membranes on soft polymer cushions: fabrication, characterization, and applications. Trends Biotechnol 18:58–64
Saffman PG, Delbruck M (1975) Brownian motion in biological membranes. Proc Natl Acad Sci USA 73:3111–3113
Safinya CR, Sirota EB, Roux D, Smith GS (1989) Universality in interacting membranes: the effect of cosurfactants on the interfacial rigidity. Phys Rev Lett 62:1134–1137
Safran SA (1983) Fluctuations of spherical microemulsions. J Chem Phys 78:2073–2076
Safran SA (1994) Statistical thermodynamics of surfaces, interfaces and membranes. Westview Press, Boulder

Saxton MJ (1989) The spectrin network as a barrier to lateral diffusion in erythrocytes: a percolation analysis. Biophys J 55:21–28
Saxton MJ (1990a) The membrane skeleton of erythrocytes: a percolation model. Biophys J 57:1167–1177
Saxton MJ (1990b) The membrane skeleton of erythrocytes: models of its effect on lateral diffusion. Int J Biochem 22:801–809
Saxton MJ (1995) Single-particle tracking: effects of corrals. Biophys J 69:389–398
Schindler M, Koppel DE, Sheetz MP (1980) Modulation of protein lateral mobility by polyphosphates and polyamines. Proc Natl Acad Sci USA 77:1457–1461
Schneider M, Jenkins J, Webb W (1984) Thermal fluctuations of large quasi-spherical bimolecular phospholipid-vesicles. J Phys (Paris) 45:1457
Seifert U (1994) Dynamics of a bound membrane. Phys Rev E 49:3124–3127
Seifert U, Lipowsky R (1995) Morphology of vesicles. In: Lipowsky R, Sackmann E (eds) Structure and dynamics of membranes, vol 1. Elsevier, Amsterdam
Seifert U, Berndl K, Lipowsky R (1991) Shape transformations of vesicles: phase diagram for spontaneous-curvature and bilayer-coupling models. Phys Rev A 44:1182–1202
Sheetz MP (1983) Membrane skeletal dynamics: role in modulation of red blood deformability, mobility of transmembrane proteins and shape. Sem Hematol 20:175–188
Sheetz MP, Schindler M, Koppel DE (1980) The lateral mobility of integral membrane proteins is increased in spherocytic erythrocytes. Nature 285:510–512
Shelley JC, Shelley MY (2000) Computer simulation of surfactant solutions. Curr Opin Colloid Interface Sci 5:101–110
Shelley JC, Shelley MY, Reeder RC, Bandyopadhyay S, Klein ML (2001) A coarse grain model for phospholipid simulations. J Phys Chem B 105:4464–4470
Shillcock J, Lipowsky R (2002) Equilibrium structure and lateral stress distribution of amphiphilic bilayers from dissipative particle dynamics. J Chem Phys 117:5048–5061
Singer SJ, Nicolson GL (1972) The fluid mosaic model of the structure of cell membranes. Science 175:720–731
Sintes T, Baumgärtner A (1998a) Interaction of wedge-shaped proteins in flat bilayer membranes. J Phys Chem B 1998:7050–7057
Sintes T, Baumgärtner A (1998b) Membrane-mediated protein attraction. a Monte-Carlo study. Physica A 249:571–575
Smit B, Hilbers P, Esselink K, Rupert L, van Os N, Schlijper AG (1991) Structure of a water oil interface in the presence of micelles—a computer simulation study. J Phys Chem 95:6361
Smith G, Sirota E, Safinya C, Clark N (1988) Structure of the l_β phases in a hydrated phosphatidylcholine multimembrane. Phys Rev Lett 60:813–816
Smith G, Sirota E, Safinya C, Plano R, Clark N (1990) X-ray structural studies of freely suspended ordered hydrated dmpc multimembrane films. J Chem Phys 92:4519–4529
Smondyrev AM, Berkowitz ML (1999) Structure of dipalmitoylphosphatidylcholine/cholesterol bilayer at low and high cholesterol concentrations: molecular dynamics simulation. Biophys J 77:2075–2089
Soddemann T, Dunweg B, Kremer K (2001) A generic computer model for amphiphilic systems. Eur Phys J E 6:409–419
Stadler C, Schmid F (1999) Phase behavior of grafted chain molecules: influence of head size and chain length. J Chem Phys 110:9697
Steck TL (1989) Red cell shape. In: Stein W, Bronner F (eds) Cell shape: determinants, regulation and regulatory role. Academic, New York, pp 205–246
Stevens MJ (2004) Coarse-grained simulations of lipid bilayers. J Chem Phys 121:11942
Tien HT, Ottova-Leitmannova A (2003) Planar lipid bilayers (BLMs) and their applications. Elsevier, Amsterdam
Tobias DJ, Tu KC, Klein ML (1997) Atomic-scale molecular dynamics simulations of lipid membranes. Curr Opin Colloid Interface 2:15–26
Tomishige M, Sako Y, Kusumi A (1998) Regulation mechanism of the lateral diffusion of band 3 in erythrocyte membranes by the membrane skeleton. J Cell Biol 142:989–1000
Tsuji A, Ohnishi S (1986) Restriction of the lateral motion of band 3 in the erythrocyte membrane by the cytoskeletal network: dependence on spectrin association state. Biochemistry 25:6133–6139
Tsuji A, Kawasaki K, Ohnishi S, Merkle H, Kusumi A (1988) Regulation of band 3 mobilities in erythrocyte ghost membranes by protein association and cytoskeletal meshwork. Biochemistry 27:7447–7452
Venturoli M, Smit B, Sperotto MM (2005) Simulation studies of protein-induced bilayer deformations, and lipid-induced protein tilting, on a mesoscopic model for lipid bilayers with embedded proteins. Biophys J 88:1778–1798
Wang Z, Frenkel D (2005) Modeling flexible amphiphilic bilayers: a solvent-free off-lattice Monte Carlo study. J Chem Phys 135:234711
Weikl TR, Lipowsky R (2000) Local adhesion of membranes to striped surface domains. Langmuir 16:9338–9346
Weis J, Levesque D, Zarragoicoechea G (1992) Orientational order in simple dipolar liquid-crystal models. Phys Rev Lett 69:913–916
Weiss TM, van der Wel PC, Killian JA, Koeppe RE, Huang HW (2003) Hydrophobic mismatch between helices and lipid bilayers. Biophys J 84:379–385
Whitehead L, Edge CM, Essex JW (2001) Molecular dynamics simulation of the hydrocarbon region of a biomembrane using a reduced representation model. J Comput Chem 22:1622–1633
Yamamoto S, Maruyama Y, Hyodo S-A (2002) Dissipative particle dynamics study of spontaneous vesicle formation of amphiphilic molecules. J Chem Phys 116:5842–5849
Zangi R, Rice SA (2003) Freezing transition and correlated motion in a quasi-two-dimensional colloid suspension. Phys Rev E 68:061508
Zeman K, Engelhard H, Sackmann E (1990) Bending undulations and elasticity of the erythrocyte membrane: effects of cell shape and membrane organization. Eur Biophys J 18:203–219
Zhang D, Klyatkin A, Bolin JT, Low PS (2000) Crystallographic structure and functional interpretation of the cytoplasmic domain of erythrocyte membrane band 3. Blood 96:2925–2933
Zilker A, Engelhardt H, Sackmann E (1987) Dynamic reflection interference contrast (ric-) microscopy: a new method to study surface excitations of cells and to measure membrane bending elastic moduli. J Phys (Paris) 48:2139–2151
Zilker A, Engelhardt H, Sackmann E (1992) Spectral analysis of erythrocyte flickering in the 0.3–4 μm^{-1} regime by microinterferometry combined with fast image processing. Phys Rev A 46:7998–8001
Zilman AG, Granek R (1996) Undulations and dynamic structure factor of membranes. Phys Rev Lett 77:4788–4791